Review paper

Development of β-SiAlON based ceramics for radome applications

Ibram Ganesh

Centre for Advanced Ceramics, International Advanced Research Centre for Powder Metallurgy and New Materials (ARCI), Hyderabad – 500 005, A.P., India

Received 6 August 2011; received in revised form 16 September 2011; accepted 20 September 2011

Abstract

This paper is a review article covering various methods reported on synthesis of β-SiAlON based ceramic materials and on their net-shape consolidation into radome structures. It also identifies a composition out of a wide-range β-$Si_{6-z}Al_zO_zN_{8-z}$ (where z = 0–4.1) solid solution suitable for radome applications and discusses about various efficient methods reported on fabrication of radome structures out of these compositions. This article also covers the literature pertaining to β-SiAlON-SiO_2 ceramic composites, which are considered to be materials of choice for certain high speed radome applications. Further, successful techniques employed for passivation of AlN powder against hydrolysis are also covered as this powder is one of the starting materials for both β-SiAlON and β-SiAlON-SiO_2 ceramic composites. Surface passivation of AlN is necessary as it decomposes into alumina and ammonia, when it comes into contact with water during aqueous processing of SiAlON based ceramics, thereby not permitting formation of desired SiAlON phase. Finally, the important properties of various commercial radome materials together with those of β-SiAlON and β-SiAlON-SiO_2 ceramic composites are also reviewed and presented in this article.

Keywords*: radome material, β-$Si_4Al_2O_2N_6$, β-SiAlON-SiO_2 composite, near-net shape consolidation*

Contents

* Corresponding author: tel: +91 40 24442699,
e-mail: *ibramganesh@arci.res.in*, *ibram_ganesh@yahoo.com*

I. Introduction

1.1 Material selection for radome applications

Development of ceramic materials for radome applications has been the topic of numerous recent investigations and this area of research has received a great deal of attention from materials scientific community [1–21]. Certain missiles that travel at a speeds grater than Mach 5 see a transient temperature of about 1370°C together with high mechanical and aero-thermal loads [1–5]. To withstand these severe environments while transmitting electromagnetic RADAR signals without any disturbance, the materials used for construction of radomes for these high speed missile applications should possess a low dielectric constant, a low loss tangent, a high flexural strength, high thermal shock resistance, high rain erosion and particle impact resistance together with high elastic modulus to keep the thin walls of radomes from buckling [1–13]. A great variety of materials such as, Pyroceram 9606 [2–5], Rayceram 8 [2–5], fused silica [7], barium aluminium silicate (BAS) [8,9], aluminium phosphate (commercially known as Cerablak™ and manufactured by Applied Thin Films, Inc., Evanston, IL, USA) [10,11], SiO_2-AlN ceramics [12], SiO_2-BN ceramics [13], reaction-bonded silicon nitride [14], liquid-phase sintered silicon nitride [15,16], silicon nitride nano-composite (Si_2N_2O, which is also called as SiON) [17], β-$Si_4Al_2O_2N_4$ [2–5,18–20], β-$Si_4Al_2O_2N_4$-SiO_2 ceramic composite [1,21], etc., have been investigated so far for these applications. Although all these types of materials have been investigated for these applications only a few materials (as listed in Table 1) have received considerable importance. It can be seen from this table that fused silica possesses excellent dielectric properties (a dielectric constant of 3.9 at 20°C and 4.1 at 1000°C and a loss tangent of 0.0001 at 20°C and <0.01 at 1000°C) making it an ideal material for radome applications [7]. However, its inferior strength (40–50 MPa) and limited withstanding of high temperatures (<800°C) restrict its use for only certain low speed radome applications. In addition to this, silicon nitride nano-composite (Si_2N_2O or SiON) also possesses good dielectric properties but preparing it with consistent properties repeatedly is not possible as its final chemical composition does not depend on the starting precursor materials composition, but instead depends on the extent of oxidation of α-Si_3N_4 powder that occurs upon calcination in an air atmosphere [6]. The oxidation behaviour of α-Si_3N_4 powder is known to be quite sensitive to several processing parameters such as, atmospheric humidity, the degree of agglomeration of powder particles, temperature fluctuations in furnace, etc. Although, dense sintered silicon nitride possesses exceptionally high flexural strength at room (600–1000 MPa) as well as at high temperatures and withstanding capability together with reasonably acceptable dielectric properties, the major drawback of this material is its poor sintering ability, which requires hot pressing (HP)/hot isostatic pressing (HIP) to achieve desired densification. Nevertheless, the pure Si_3N_4 ceramics cannot be densified under pressureless sintering conditions without using large amount of certain sintering aids. The radome structures consolidated with near-net shape following certain cost-effective techniques like gel-casting cannot be sintered without disturbing the radome structure using HP/HIP techniques. Similarly, silicon nitride-barium aluminium silicate (Si_3N_4/BAS) composite also possesses reasonably high flexural strength (420 MPa) but preparation of radome structures out of this material was found to be quite cumbersome [8]. The only material that can be shaped into radome structures following near-net shape forming techniques like aqueous gelcasting and can also be sintered to full density without disturbing its radome structure is β-SiAlON [2–5]. In the fabrication of β-SiAlON radomes, an aqueous suspension containing required amounts of precursor

Table 1. Commonly employed radome materials and their main characteristics

Material	Fused silica	Silicon nitride based ceramics			
Phase	SiO_2 (amorphous)	Si_3N_4	β-SiAlON	Si_3N_4 / BAS[$]	Si_2N_2O
Temperature withstanding capability [°C]	<800	>1300	>1300	>1300	>1300
Strength [MPa]	40-50	600-1000	266	420	190
Dielectric constant, *k* (20°C)	3.9	7.96	6.84-7.46	7.50	4.80
Dielectric constant, *k* (1000°C)	4.01	8.59	7.34	8.16	5.02
Loss tangent, *tan δ* (20°C)	0.001	0.008	0.0013-0.002	-	0.0014
Loss tangent, *tan δ* (1000°C)	<0.01	0.013	0.003-0.004	-	0.0025
Processing route	Slip casting + moderate machining	*	‡	†	

* Require hot isostatic pressing (HIP) or hot pressing (HP) followed by extensive diamond grinding

‡ Colloidal processing to near net shape, green machining followed by sintering and final limited diamond grinding / lapping

† Controlling chemical composition is very difficult.

$ Barium aluminium silicate

materials (i.e. α-Si_3N_4, α-Al_2O_3, SiO_2 and AlN together with certain sintering aids such as Y_2O_3) is consolidated in non-porous moulds followed by drying and reaction sintering at elevated temperatures in nitrogen atmosphere [2,22].

Nevertheless, there are two critical issues, which need to be resolved before attempting to fabricate β-SiAlON radomes with near-net shape [18–21]. The first one is fixing of right chemical composition based on the best combination of physical, thermal, dielectric and mechanical properties out of a wide-range of β-$Si_{6-z}Al_zO_zN_{8-z}$ (where z = 0-4.1) solid solution [23]. Furthermore, this composition needs to undergo full densification under pressureless sintering conditions [18–21]. The second one is establishment of suitable net-shape forming technique for making radome structures with desired product yields [19,22]. It is known that processing of β-SiAlON ceramics following aqueous colloidal processing routes is quite difficult as AlN, one of the essential precursor materials of β-SiAlON ($(6-z)Si_3N_4 + zAl_2O_3 + zAlN \leftrightarrow 3Si_{6-z}Al_zO_zN_{8-z}$, where $0 \leq z \leq 4.1$) decomposes into alumina and ammonia during aqueous processing ($AlN + 3H_2O \rightarrow Al(OH)_3 + NH_3$) [25]. Despite this problem, Janney *et al*. [2], and Kirby *et al*. [3–5], at Oak Ridge National Laboratory (ORNL), USA, could fabricate β-$Si_4Al_2O_2N_6$ radomes successfully by utilizing a commercially obtained water processable AlN powder [2]. Furthermore, these radomes were successfully test fired for certain missile applications after sintering [3–5]. Nevertheless, this water processable AlN powder is scarce in the open market. In addition to this, the basis for selecting β-$Si_4Al_2O_2N_6$ composition by ORNL for these radome applications was not revealed [2]. On the other hand, the dielectric constant (~7.3) of β-$Si_4Al_2O_2N_6$ is also found to be on the higher side for use in radomes for certain high speed vehicles [1–15]. This high dielectric constant value demands the wall thickness of the sintered β-$Si_4Al_2O_2N_6$ radome to be fixed to ≤3.5 mm in order to transmit the electromagnetic waves (i.e., RADAR signals) in the microwave range (~17 GHz) without any disturbance [1–15]. However, fabrication of one meter long radomes with about 3.3 mm thickness was found to be a difficult task [2–5]. Most of the commercially available radomes have wall thickness of at least 5 mm. To make 5 mm thick β-$Si_4Al_2O_2N_6$ radomes, the dielectric constant of β-$Si_4Al_2O_2N_6$ should be reduced to ≤6 while maintaining its flexural strength >100 MPa [6–17]. In order to confer such properties to this material, many efforts were made to introduce the low dielectric constant SiO_2 into β-SiAlON matrix [1,18–20]. Nevertheless, β-$Si_4Al_2O_2N_6$-SiO_2 ceramic composites with >9 wt.% SiO_2 cannot be prepared by following any conventional powder processing route using α-Si_3N_4, α-Al_2O_3 and AlN as precursor materials [18–20]. This is due to the fact that when >9 wt.% SiO_2 is to be introduced into SiAlON matrix, in addition to α-Si_3N_4, α-Al_2O_3 and AlN, an additional SiO_2 is required as an additional precursor material. This additional SiO_2 increases the diffusion paths between reactive Si^{4+} and Al^{3+} species during sintering that restricts the formation of desired amount of β-SiAlON phase, which is very important to realize high flexural strength for β-$Si_4Al_2O_2N_6$-SiO_2 ceramic composite [23].

In a study, Gilde *et al*. [6] prepared a silicon oxynitride (Si_2N_2O or SiON) nano-composite by calcining α-Si_3N_4 powder in an open-air atmosphere at 1700°C followed by sintering of this calcined α-Si_3N_4 powder compact in nitrogen atmosphere at >1800°C. However, in this process the final product could not be prepared repeatedly with consistent properties as mentioned in the first paragraph. In another study, Ganesh *el al*. [18] successfully synthesized β-$Si_4Al_2O_2N_6$-9.0 wt.% SiO_2 composite by following a reaction sintering process in which a compacted mixture of silicon nitride and alumina was treated at 1750°C for 4 h under ~101.63 kPa N_2 atmosphere using 7 wt.% Y_2O_3 as a sintering aid (i.e. 1.5 $Si_3N_4 + Al_2O_3 \rightarrow$ β-$Si_4Al_2O_2N_6$ + 0.5 SiO_2 (i.e. 9 wt.% SiO_2)). However, none of the compositions of α-Si_3N_4, α-Al_2O_3 and AlN precursors yielded β-$Si_4Al_2O_2N_6$ with > 9 wt.% SiO_2. Lately, Advanced Materials Organization, Inc., USA, has started producing ceramic composites with a chemical composition of 70 wt.% SiAlON + 30 wt.% fused silica in the form radomes of 25 cm height and 17.8 cm base diameter for certain high speed radome applications [1]. In this process, initially, a green radome was fabricated following a non-aqueous gelcasting of a suspension containing β-SiAlON precursor mixture + 30 wt.% organic fugitive material. After drying, this gelcast green radome was sintered for 2–4 h at >1750°C under a N_2 pressure of 50–100 bar to obtain radome with a porosity of about 30% (porosity is formed due to the burning out of the added fugitive material). To fill the generated porosity, fused silica was infiltrated by plasma spraying technique. Fused silica is mainly added to reduce the dielectric constant as well as the density of radome from 3200 kg/m^3 to 2200 kg/m^3, which is recommended for the above mentioned high speed radome applications [1,6]. Preparation of β-SiAlON radomes with >30 wt.% fused silica following this route is associated with several practical problems, as it is required to create >30% porosity in the sintered radome. Making one-meter long radomes with >30% porosity is not an easy step. Additionally, this process has been found to be very laborious and needs highly capital-intensive equipment. Therefore, a simple route for preparing different types of β-SiAlON-SiO_2 ceramic composites with SiO_2 content in the range from 20 to 80 wt.% is highly desired in order to have composites with <6 dielectric constant and >100 MPa strength for the intended applications [21,26].

1.2 Surface passivation of AlN powder against hydrolysis

As, AlN is one of the starting materials for β-SiAlON and β-SiAlON-SiO_2 ceramic composites, in order to fabricate radome structures out of these materials with near-net shape following aqueous colloidal processing routes, it is very much necessary to passivate AlN powder against hydrolysis [2–5,18–21]. Otherwise, AlN decomposes during aqueous processing of SiAlONs leading to the coagulation and eventual setting up of the aqueous colloidal slurry in the vessel used for powder de-agglomeration operation thereby not permitting the formation of the targeted final SiAlON composition [2,22]. Owing to the scarcity of water processable AlN powder in the open market, and due to the presence of the hydrophobic substances as coatings on the surfaces of those commercially available water processable AlN powders which hinder achieving high solids loading (>50 vol.%) in particulate (colloidal) suspensions required for net shape consolidation of thin wall radomes, there were several efforts to develop simple and effective techniques to passivate AlN powder against hydrolysis using materials having hydrophilic groups [27–30]. In one study, a di-carboxylic acid (sebacic acid) was utilized to facilitate hydrophilic groups on the surface of treated AlN powder while protecting it against hydrolysis [27]. In another study, aluminium di-hydrogen phosphate, $Al(H_2PO_4)_3$, was employed to provide a stable phosphate layer on the surface of AlN powder in the aqueous media at pH ~1–3 [28,29]. Yet in another study, a SiO_2 coating was provided on AlN powder in vacuum at 1150–1450°C to protect AlN from hydrolysis [30]. However, all of these processes involve either meticulous control of processing parameters or tedious procedures, thereby making the processes not only complicated but also adversely affecting the environment and the economy of the processes [30–32]. Hence, there is still an open quest to develop ever simpler methods to passivate AlN powder against hydrolysis so that it can be employed in aqueous processing of SiAlON based radome shapes with near-net shape [18–21].

1.3 Near-net shape consolidation of β-SiAlON radome structures

On account of their several useful properties such as, high strength, good oxidation and creep resistance at ambient and elevated temperatures, high elastic modulus, good thermal shock resistance and outstanding rain erosion, particle impact resistance, etc., β-SiAlON ceramics were employed for several applications including radomes for certain high speed missiles [33–40]. β-SiAlON components for these applications are normally fabricated by following a conventional dry-powder pressing (CDPP) of precursor mixtures and then reaction sintering of these compacted precursor mixtures at elevated temperatures in nitrogen atmosphere to achieve the desired density followed by an extensive and expensive machining to obtain the targeted final shape [33–40]. However, this CDPP technique was found to be quite expensive particularly for making large size and complex-shaped components like turbine rotors and radomes. In order to reduce the processing cost of these components, techniques like slip casting [38], injection moulding [39], temperature induced forming [40], etc., have been tried. However, the productivity and green strength of the parts obtained in these routes have been found to be un-satisfactory. Furthermore, as the forming technique directly impacts the productivity, the ultimate quality and the cost of the manufactured products, particularly in the case of mass production of several advanced ceramics, high productivity with minimum cost must be fulfilled. In view of these reasons, efforts are still needed to be focused on developing simpler and cheaper technologies for processing of β-SiAlON components with near-net shape [19,21,22].

As described by Prof. Evans in a classic review article [41], there are as many as seventy different ways to make ceramic components. Among these numerous ways, only a few methods including powder injection moulding (PIM) [42–47], solid freeform fabrication (SFF) [48–51], and selective laser sintering (SLS) [52–57] have received considerable importance for fabricating certain intricate shaped ceramic products in large quantity on a commercial scale. The efficacy of PIM method was established by German [42–44] as well as by Evans and Edirisinghe [45–49] separately for a great variety of ceramic materials. Although this method has been effectively employed to fabricate certain high end components such as silicon carbide turbochargers and radial rotors for heat engines, alumina thread guides, rare earth magnet pole pieces for hard disk drives, stainless steel gear wheels for electric tooth brushes, etc., it is yet to be tested for manufacturing of large SiAlON radome structures [42–47]. As rightly pointed out by Edirisinghe [49,50] and others [51], the solid freeform fabrication (SFF) is a genus of the manufacturing processes that has been practiced for the fabrication of several three-dimensional ceramic components by assembling their starting materials by point, line or plane. This process has certain advantages over other related processes such as, i) non requirement of any tooling or machining, ii) a dramatic reduction in the time and cost of each design iteration, particularly the first, iii) rapid production of a prototype that could save significant amounts of time and money, iv) dramatic speed up of the entire cycle of designing and bringing a new product to market, v) utilization of a computer aided design (CAD) file to fabricate ceramic components layer by layer, etc.. Nevertheless, this process is yet to be proved for the manufacturing of large SiAlON radome structures [58]. Of late, selective laser sintering (SLS) has also

received a great deal of attention by ceramic community in the manufacturing of near-net shape ceramic components with very high dimensional precision and considerably lower processing times [52–57]. Song *et al*. [52] established a theoretical basis for this process for fabricating three dimensional ceramic components out of several ceramic materials including alumina [55], alumina-zirconia [56], Al_2O_3/SiO_2 composite ceramics [57], and yttria-zirconia. However, this process has not been utilized so far in the manufacturing of SiAlON radome structures [58].

It is a well-known fact that aqueous colloidal processing routes offer several environmental and economic benefits apart from the ability to manipulate inter particle forces in aqueous suspensions [2,22,58–67]. On the other hand, as the fracture in the ceramic materials originates from micro-structural imperfections such as pores and inclusions, and leads to poor mechanical reliability, effective de-agglomeration of the powder particles in the slurries is essential. During 1990 period, aqueous gelcasting (GC) has been identified as one of the most efficient near-net-shaping routes, which confers relatively high strength to the green consolidates [2,22]. Furthermore, the green strength of the gelcast part has been found to be three-to-four times higher as compared with that of the compact made by CDPP route [2,22]. However, the drying procedure involved in this process does not allow obtaining crack free green components due to differential shrinkages, particularly when they have different wall thicknesses at different places like in radomes (i.e., nose and wall) [19]. On the other hand, during the same time period, hydrolysis assisted solidification (HAS) has also been identified as a simple and inexpensive net-shaping route that has been employed to consolidate several kinds of ceramics in which alumina is a major or minor constituent [25]. In this process, aluminium hydroxide ($AlN + 3H_2O \rightarrow Al(OH)_3 + NH_3$) formed by the hydrolysis of AlN which is added to the suspension to promote setting/gelling process acts as cement conferring a relatively high stiffness to the green consolidates. This in turn, keeps the shape of the part intact upon further drying and binder removal operations, thereby minimizing the expensive post-sintering machining operations. Additionally, as this process is not driven by any externally applied pressure or water absorption by an absorptive mould like in the slip casting, it effectively utilizes various thermally activated chemical processes *in situ*. However, the thin wall ceramic components are difficult to fabricate following this process as green parts formed by this method were found to be very brittle [25,59].

In 2009, a new near-net-shaping technique named hydrolysis induced aqueous gelcasting (GCHAS) [19,21,60–63] was successfully developed to address the problems associated with GC and HAS processes. GCHAS is a combination of aqueous gelcasting (GC) and hydrolysis assisted solidification (HAS) processes. Different kinds of ceramics (β-$Si_4Al_2O_2N_6$ [19], ZTA [60], $MgAl_2O_4$ [61,62], and Al_2O_3 [63]) consolidated by GCHAS route exhibited significantly higher green strengths in comparison to those consolidated by any other existing technique including original individual techniques GC and HAS. The synergetic effects of the these two latter processes are quick setting of the suspension into a stiff gel under ambient conditions with an exceptionally high strength and an absence of differential shrinkage during drying, and thus avoiding cracking of the part. This is a consequence of water being partially consumed by the hydrolysis of AlN ($AlN + 2H_2O \rightarrow AlO(OH) + NH_3$) added to the suspension for room temperature consolidation purpose. The concomitant increase in pH of the system can also favourably change the permeability of the green bodies and minimise the thermal/moisture gradients. These advantages in turn enable fabrication of defect free thick, thin and relatively large components of all ceramics that contain Al_2O_3 as a major or minor component and that utilize and/or tolerate Al_2O_3 as a sintering aid [19,21,60–63].

Considering the importance of net shape consolidation of β-SiAlON and β-SiAlON-SiO_2 radomes for certain high-speed missile applications, a systematic study was undertaken recently while keeping the following objectives in mind. i) identification of the best β-SiAlON composition out of a wide-range β-$Si_{6-z}Al_zO_zN_{8-z}$ (where $z = 0 – 4.1$) solid solution based on the physical, dielectric and mechanical properties and the possibility to be sintered to full density under pressureless sintering conditions [42]; ii) development of a simple surface treatment technique for passivating AlN powder against hydrolysis [31,32]; iii) development of a simple powder processing route for preparing dense β-$Si_4Al_2O_2N_6$-SiO_2 ceramic composites with SiO_2 in the range of 20–80 wt.% [21,26]; and iv) development of an efficient and simple technique for fabricating β-$Si_4Al_2O_2N_6$ and β-$Si_4Al_2O_2N_6$-SiO_2 radome structures with near-net shape and with very high product yield [19,21,60–63]. The results published in the literature to address these objectives are reviewed, presented and discussed in this article.

II. Experimental section

The simple and effective experimental procedures reported in the literature on synthesis and net-shape consolidation of β-SiAlON and β-SiAlON-SiO_2 ceramic composite radomes, and for surface passivation of AlN powder against hydrolysis are briefly presented in this experimental section.

2.1 Surface passivation of AlN powder

As purchased AlN powder (hereafter termed as A-AlN) could be passivated against hydrolysis following a simple surface treatment method [31,32]. In a

typical experiment, about 175 mL absolute ethanol (99.9%, Les Alcools De Commerce Inc., Ontario) was taken in a 500 mL three-neck round bottom (RB) flask (Duran, India), which was fitted with a condenser, equalization (dropping) funnel and an adopter for passing dry-nitrogen gas from a pressure cylinder. The RB flask was fixed in an oil-bath (the glass dish had 150 mm diameter and 75 mm height, Biotek-Scientific, Hyderabad, containing furnace oil (Thermol-100, –50° to +250°C, Biolabs, Hyderabad, India)). The entire set-up was fixed on a magnetic stirrer (5MLH-DX, Remi, India). About 245 g of A-AlN powder was slowly introduced into ethanol present in a RB flask to obtain ~250 cm^3 30 vol.% solids loaded slurry. In a separate experiment, ~2 g $Al(H_2PO_4)_3$ was digested in ~5 mL of hot H_3PO_4. This solution was then mixed with ~50 mL ethanol and added drop-by-drop to the alcoholic AlN solution (RB flask contents) with the help of an equalization funnel. After completing the addition process, the RB contents were continuously refluxed at 80°C for 24 h while passing nitrogen gas from a pressure cylinder at a rate of 100 cm^3/min. The treated AlN slurry was filtered off and washed with fresh ethanol several times in order to remove any un-reacted/excess H_3PO_4 acid and $Al(H_2PO_4)_3$ from the surface of the treated powder [31,32]. The washing process was continued until the pH of the washed ethanol reached the pH of the fresh ethanol. This powder was then dried at 80°C in an electrically heated oven (Lindberg Blue, USA) over night. The ethanol was repeatedly used several times after subjecting it to the distillation process. Hereafter, the treated powder is termed as T-AlN. The main advantages of this non-aqueous surface passivating process are: i) the formation of a single uni-molecular phosphate monolayer, ii) the excess un-reacted coating agents can be washed away from the powder surface with ethanol, and iii) the ethanol used for washing purpose can be re-used several times after subjecting it to a conventional distillation process. This differs from the existing aqueous acidic solution processing routes that require an excess of H_3PO_4 or $Al(H_2PO_4)_3$ that will remain on the powder surface [31,32].

2.2 Preparation of dense ceramics by conventional dry-powder pressing (CDPP) route

A conventional dry-powder pressing (CDPP) technique was employed to make different types of dense β-SiAlON ceramics and the β-SiAlON-SiO_2 ceramic composites [21,22,24]. The suppliers' details and some of the characteristics of the precursor materials used for the preparation of these β-$Si_{6-z}Al_zO_zN_{8-z}$ (z = 1, 1.5, 2, 2.5, 3, 3.5 & 4) ceramics are presented in Table 2. For preparing β-SiAlON-SiO_2 (SiO_2 = 0, 20, 40, 50, 60, 80 & 100 wt.%) ceramic composites, a commercial fused silica powder and a β-$Si_4Al_2O_2N_6$ powder obtained in a conventional extrusion process followed by reaction sintering were used as the starting raw materials [22]. Prior to pressing into pellets of 30 or 90 mm diameter × ~10 mm height under a pressure of about 200 MPa, ~200 g precursor powders mixtures of both β-SiAlON ceramics and β-SiAlON-SiO_2 ceramic composites (each composition at a time), ~60 g of 5 wt.% aqueous PVA solution and ~200 g of ZrO_2 cylindrical pebbles (10 mm diameter and 12 mm length) were suspended in ~200 mL of toluene in a 500 mL alumina bowl and were ground for 30 min in a planetary ball mill (Retsch, GmbH, Germany) by maintaining 200 rpm. The resultant dough was separated from toluene, dried at ~90°C for 12 h in an electrically heated oven and passed through a –30 BSS mesh to obtain granules with less than 595 μm prior to pressing into pellets. Binder burnout was operated at 500°C for 1 h prior to sintering at 1675–1700°C for 3–4 h in nitrogen atmosphere (~800–1100 torr) [19,21,24]. During sintering, these pellets were covered with 50 wt.% Si_3N_4 + 50 wt.% BN to protect them from decomposition and/or deformation.

2.3 Preparation of β-$Si_4Al_2O_2N_6$ powder by conventional extrusion method

In order to use it as one of the starting materials for preparing β-SiAlON-SiO_2 ceramic composites, the β-$Si_4Al_2O_2N_6$ powder was synthesized by reaction sintering of extrudates containing a powder mixture of 64.33 wt.% α-Si_3N_4, 23.36 wt.% α -Al_2O_3, 9.37 wt.% AlN (surface passivated against hydrolysis) and 7 wt.% Y_2O_3 (Table 2) at 1675°C for 4 h in N_2 atmos-

Table 2. The details of suppliers and the characteristics (BET surface area and average particle size values and the XRD phases) of various raw materials employed to consolidate β-$Si_4Al_2O_2N_6$ and β-SiAlON-SiO_2 ceramic composites

Raw material	Supplier and grade of the raw material	BET SA [m^2/g]	Average particle / agglomerate size [μm]	XRD phase
α-Al_2O_3	HP Grade, ACC India Limited, India	1.24	1.39	Corundum
α-Si_3N_4	SicoNide-P95H, VESTA Ceramics AB, Sweden	17.77	6.51	α-Si_3N_4
Y_2O_3	Rhodia Inc., Phoenix, Arizona, USA	3.41	3.23	Y_2O_3
AlN	Grade AT, H.C. Stark, Germany	6.72	7.62	AlN
Fused silica	Chettinad Quartz Products Private Ltd., Chennai, India	-	19.95	Amorphous fused silica

phere [21,22]. In a typical experiment, the required amounts of precursor powders mixture was kneaded in a conventional dough making machine (Sigma Kneader, Prigmayers India Private Limited, India) with 3 wt.% methyl cellulose, 2 wt.% polyethylene glycol (PEG 400) (both are GR grade procured from Loba Chemie, Mumbai, India) and about 30 wt.% double distilled water to obtain an easily extrudable dough [68]. The resultant dough was then extruded through an indigenously designed and fabricated stainless steel die using a ram type extruder at a rate of 50 mm min^{-1} under a pressure of 10–20 kg/cm^2 to form extrudates of about 5 mm thickness [68]. These extrudates were allowed to dry in an open-air atmosphere over night under ambient conditions, which were then cut into 5–6 mm length pieces. These cut pieces were then subjected to binder removal for 2 h at 500°C and then sintered for 4 h at 1675°C under a N_2 atmosphere of about 800 torr to form β-$Si_4Al_2O_2N_6$ extrudates [19]. During sintering, these extrudates were covered with a powder mixture consisting 50 wt.% Si_3N_4 + 50 wt.% BN to protect them against decomposition [18–22]. The sintered extrudates were crushed in a hammer mill followed by wet-grinding in a stainless steel jar (350 mm diameter and 400 mm height) using stainless steel balls with diameters of about 12 mm and 25 mm while maintaining 1:8 weight ratio of charge to balls. This milling operation was continued until the average particle size of β-$Si_4Al_2O_2N_6$ was around 3 μm [22]. From the resultant ground powder, the iron contamination was removed with the help of several magnets having dimensions of 30 mm diameter and 10 mm height.

2.4 Net-shape consolidation of β-$Si_4Al_2O_2N_6$ and β-SiAlON-SiO_2 ceramics by colloidal processing routes

The precursor mixture compositions employed for consolidating β-$Si_4Al_2O_2N_6$ and β-$Si_4Al_2O_2N_6$-9 wt.% SiO_2 composite ceramics by following different routes are summarized in Table 3. For the sake of an easy identification, different codes are given to denote these precursor mixture compositions. CDPP stands for conventional dry-powder pressing; GC stands for aqueous gelcasting; HAS stands for hydrolysis assisted solidification; GCHAS stands for hydrolysis induced aqueous gelcasting; SSC9 stands for β-$Si_4Al_2O_2N_6$-9 wt.% SiO_2 ceramic composite. Except for SSC9, all other samples' targeted chemical composition was β-$Si_4Al_2O_2N_6$. In the sample codes numbers (2–10) represent the amount of A-AlN in the precursor mixture, which would hydrolyze ($AlN + 3H_2O \rightarrow Al(OH)_3 + NH_3$) in the slurry after casting in the non-porous moulds and the T-AlN stands for AlN powder surface treated against hydrolysis. The experimental procedures involved in consolidation of β-$Si_4Al_2O_2N_6$, β-$Si_4Al_2O_2N_6$-9 wt.% SiO_2 and 60 wt.% β-SiAlON + 40 wt.% SiO_2 ceramic composites by GC, HAS and GCHAS are presented briefly in the following sections.

2.4.1 Aqueous gelcasting (GC)

In a typical experiment, a precursor mixture (GC-SSC9 or GC, Table 3) was suspended in a premix solution, which has been prepared by dissolving either 20 wt.% methacrylamide (MAM), mithylenebisacrylamide (MBAM) and n-vinylpyrrolidinone (NVP) in 3:1:3 ratio (termed as nonconventional premix solution, NCPM) or 17 wt.%

Table 3. Precursor mixtures used for preparing β-$Si_4Al_2O_2N_6$ ceramics and β-$Si_4Al_2O_2N_6$-9 wt.% SiO_2 ceramic composite by following a conventional dry-powder pressing (CDPP), aqueous gelcasting (GC-SSC9 and GC), hydrolysis assisted solidification (HAS-5 to HAS-15) and hydrolysis induced aqueous gelcasting (GCHAS-2 to GCHAS-10) techniques [19]

Sample code†	α-Si_3N_4 [wt.%]	A-AlN [wt.%]	α-Al_2O_3 [wt.%]	Y_2O_3 [wt.%]	T-AlN [wt.%]
CDPP	64.33	9.37	23.36	7	-
GC-SSC9	62.77	-	30.22	7	-
HAS-5	64.33	5	18.36	7	9.37
HAS-10	64.33	10	13.36	7	9.37
HAS-15	64.33	15	8.36	7	9.37
GC	64.33	0	23.36	7	9.37
GCHAS-2	64.33	2	21.36	7	9.37
GCHAS-5	64.33	5	18.36	7	9.37
GCHAS-7	64.33	7	13.36	7	9.37
GCHAS-10	64.33	10	8.36	7	9.37

† CDPP stands for conventional dry-powder pressing; GC stands for aqueous gelcasting; HAS stands for hydrolysis assisted solidification; GCHAS stands for hydrolysis induced aqueous gelcasting; SSC9 stands for SiAlON-SiO_2 ceramic composite with 9 wt.% SiO_2; Except SSC9 (β-$Si_4Al_2O_2N_6$-9 wt.% SiO_2), all other samples' targeted chemical composition is β-$Si_4Al_2O_2N_6$. In the sample codes numbers (2-10) represent the amount of A-AlN in the precursor mixture, which would hydrolyze ($AlN + 3H_2O \rightarrow Al(OH)_3 + NH_3$) in the slurry after casting in the non-porous moulds and the T-AlN stands for AlN powder surface treated against hydrolysis.

MAS and MBAM in 6:1 ratio in de-ionized water (termed as conventional premix solution, CPM), to achieve slurries with 45–50 vol.% solids [19,58]. A commercial amino alcohol, a cationic dispersing agent (Dolapix A88, Zchimmer & Schwarz, Berlin, Germany) was employed at the ratio of 25 μL/g of powder mixture to improve the fluidity of the suspension. The resultant suspension was degassed for ~2 min after introducing an initiator (10 wt.% aqueous solution of ammonium per-sulphate, APS) and catalyst (tetramethylethylenediammine, TEMED) with the ratio of 4 and 2 μL per gram of slurry, respectively. Afterward, the slurry was cast into non-porous white petroleum jelly coated split-type aluminium moulds (60 mm×30 mm×30 mm), dried and sintered for 4 h at 1675°C in N_2 (800 torr) atmosphere. However, by following this (GC) route, the fabrication of the β-$Si_4Al_2O_2N_6$ based radomes was found to be very difficult as the formed green radomes always cracked while taking out of the mould due to their very poor strength, hence, the product yield was found to be very low (<5%) [19,58].

The precursor mixture GC-SSC9 (Table 3) leads to the formation of β-$Si_4Al_2O_2N_6$-0.5SiO_2 ceramic composite (1.5 Si_3N_4 + Al_2O_3 → β-$Si_4Al_2O_2N_6$ + 0.5 SiO_2) upon reaction sintering at elevated temperatures in N_2 atmosphere [18,19]. The 0.5 mol% silica (which is equivalent to 9.0 wt.%) formed *in situ* during the reaction reduces the dielectric constant and CTE of β-$Si_4Al_2O_2N_6$ material considerably because of its relatively low CTE (<2×10^{-6}/ºC) and dielectric constant (<4) [18]. Since, this composition does not involve AlN as one of the starting raw materials, it is relatively easy to process following aqueous gelcasting (GC) route for making β-SiAlON radomes [18,22].

2.4.2 Hydrolysis assisted solidification (HAS)

In a typical experiment, a precursor mixture of HAS-2 to HAS-15 (Table 3) was initially suspended in doubly distilled water to obtain slurries with 48 to 50 vol.% solids loading [19,58,59]. To improve the dispersion of precursor mixtures and the fluidity of the slurry, Dolapix A88 was added in a ratio of 25 μL/g of powder. All the slurries were degassed for ~5 min after milling for 16 h by vacuum pumping. All the above operations were carried out at room temperature. Afterwards, the slurries were cast into non-porous white petroleum jelly coated split-type aluminium moulds (~100/60 mm×30 mm×30 mm), which were then allowed to set under ambient conditions for about 2 h followed by a stage at ~60°C till the completion of the setting process. The green bodies thus obtained were de-moulded and dried under controlled humidity (LHL-113; Espec Corporation, Japan) conditions to avoid cracking. These dried consolidates were also sintered along with those samples consolidated by GC route. However, by following this HAS route also the β-$Si_4Al_2O_2N_6$ radomes could not be fabricated due to the very brittle nature of the green parts [19,58,59].

2.4.3 Hydrolysis induced aqueous gelcasting (GCHAS)

The hydrolysis induced aqueous gelcasting (GCHAS) process enabled successful fabrication of both β-$Si_4Al_2O_2N_6$ as well as β-$Si_4Al_2O_2N_6$-SiO_2 ceramic composite radome structures [19,21,58]. In a typical experiment, to obtain β-$Si_4Al_2O_2N_6$ or β-$Si_4Al_2O_2N_6$-SiO_2 ceramic composite based slurries, respectively, a

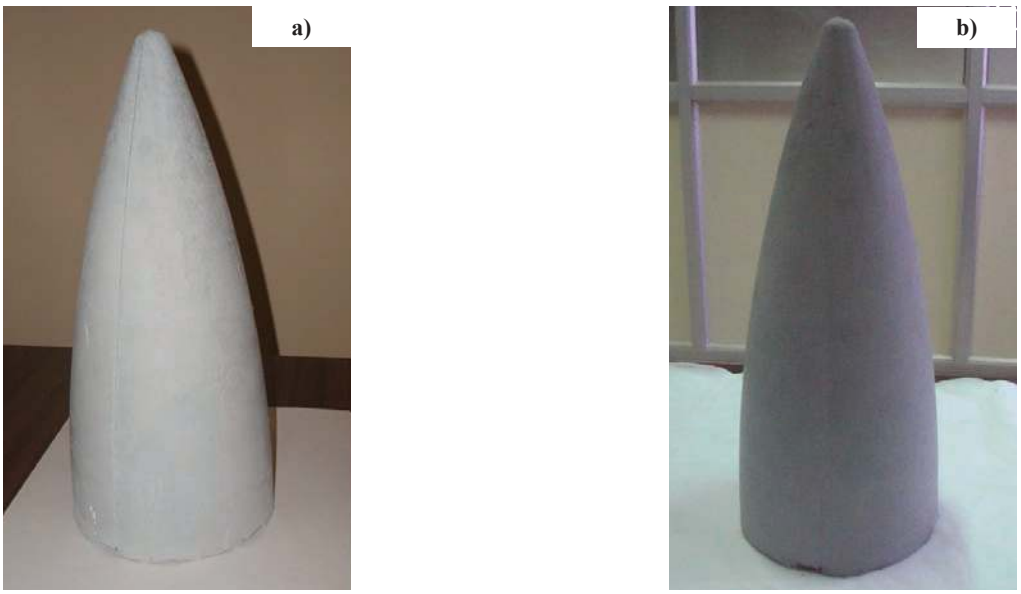

Figure 1. Photographs of green prototype radome shapes (about 290 mm height and 125 mm base diameter) consolidated by GCHAS route using (a) 50 vol.% GCHAS-5 precursor mixture (Table 3) and (b) 50 vol.% precursor mixture consisting 57.56 wt.% β-$Si_4Al_2O_2N_6$ + 38.37 wt.% fused silica + 4.06 wt.% as-purchased AlN powders, respectively

precursor mixture of GCHAS-2 to GCHAS-10 (Table 3) or a powders mixture of 60 wt.% β-$Si_4Al_2O_2N_6$ and 40 wt.% fused silica was dispersed in NCPM solution with the help of Dolapix A88 added with the ratio of 25 μL/g of powder. After mixing the resultant slurry for ~16 h, A-AlN equivalent to 1–5 wt.% of Al_2O_3 was introduced into slurry and the mixing process was continued for further ~ 2 h. The resultant slurry was filtered off and degassed for 5 min by vacuum pumping. The slurry was once again degassed for ~2 min after introducing APS and TEMED at the ratio of 4 and 2 μL per gram of slurry, respectively. These degassed slurries were then cast into an indigenously designed and fabricated split type Teflon lined aluminium radome mould, and inserted aluminium solid mandrel into the slurry. After mandrel insertion, the slurry was allowed to gel completely in the mould itself under ambient conditions [19,21,63]. The slurry was constantly poured in excess amounts in the mould so that it overflows from top of the mould in order to remove the formed air/gas bubbles (if any were left after vacuum pumping) while inserting the mandrel into the slurry in the mould. Some rectangular (60 mm×30 mm×30 mm) pieces were always cast along with radome shape to check the condition of gel before removing the mandrel from the mould [19]. After confirming the gelation of the slurry, the mandrel was removed from the mould and then filled with polyethylene glycol-400 (PEG400) (AR grade, Loba-Chemie, Mumbai, India) [21,63]. Due to high chemical potential difference, the water moves from gel (i.e., from wet radome) into PEG [2]. After about 2 h, the PEG, followed by the wet-green radome was taken out of the mould by simply tilting the mould up-side down. This wet radome was then placed in an humidity controlled oven (LHL-113; Espec Corporation, Japan), which was pre-set at 40°C and 90% RH [21,63]. Purposefully, the room temperature gelation was performed to avoid the temperature induced reactions between APS and Si_3N_4 raw material, which create a lot of porosity in the cast part, which will manifest even in the sintered parts [19,58]. After drying for 24 h at 40°C, the temperature in the humidity oven was slowly raised to 70°C and then to 90°C. At each of these temperatures the radome was held for ~ 24 h. Two prototype green radome structures formed from precursor mixture of GCHAS-5 (Table 3), and the powder composition of 57.56 wt.% β-$Si_4Al_2O_2N_6$ + 38.37 wt.% fused silica + 4.06 wt.% A-AlN, respectively, are shown in Fig. 1. The β- $Si_4Al_2O_2N_6$ based samples formed in this (GCHAS) route were sintered along with those formed in CDPP, GC and HAS routes at 1675°C for 4 h [19] and those formed from mixtures of β-$Si_4Al_2O_2N_6$ and fused silica were sintered for 3 h at 1750°C in about 900 torr N_2 pressure after subjecting them to binder burnout operation for 2 h at 500°C [21]. The radome structures were subjected to conformal sintering using graphite mandrel (Fig. 2a). A sintered and machined β-$Si_4Al_2O_2N_6$ proto-type radome is shown in Fig. 2b. The radome structures product yield in GCHAS process was found to be >95%.

2.5 Characterization

The various techniques employed to characterize the above mentioned powders, suspensions and sintered materials were described in our previously reported papers [18–26,31,59–72].

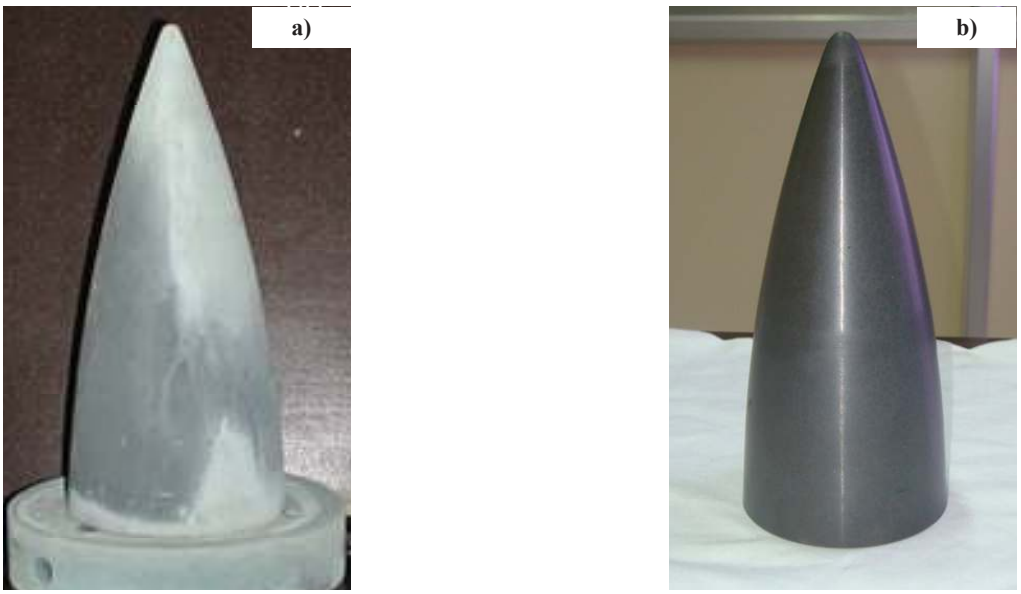

Figure 2. Photographs of (a) graphite mandrel used for conformal sintering of β-$Si_4Al_2O_2N_6$ radome structures and (b) conformal sintered (for 4 h at 1675°C in N_2 atmosphere under about 800 torr pressure) and machined β-$Si_4Al_2O_2N_6$ radome structure

III. Results and discussion

3.1 Influence of chemical composition on β-SiAlON properties

Figure 3 reveals the XRD patterns of β-SiAlON ceramics formed by reaction sintering of seven different types of precursor mixtures utilizing 7 wt.% Y_2O_3 at 1675°C for 4 h. This figure also lists different codes given to denote the ceramics [24]. In the sample codes, the numbers 1 to 4 represent the *z* value in the β-$Si_{6-z}Al_zO_zN_{8-z}$ composition and the number 7 represents the concentration of sintering aid on total powder composition basis. It can be seen that all the materials are primarily β-SiAlON ceramics ($Si_3Al_3O_3N_5$; ICDD File No. 00-036-1333 and $Si_4Al_2O_2N_6$; ICDD File No. 00-048-1616). They contain some small amounts of impurities such as, Y_2SiAlO_5N [23]. The material, Z1Y7 additionally contain some small amounts of un-reacted alumina as well. With the gradual increase of *z* value in the composition, the intensity of XRD peaks due to β-SiAlON phase is increased gradually and there is a slight shift in the 2θ values. This small shift could be attributed to the increased contents of aluminium and oxygen ions entered into β-SiAlON unit cell network. Except, Z1Y7 (84.83%) and Z1.5Y7 (88.48%), all other materials exhibited >90% β-SiAlON phase. Interestingly, none of the sintered materials exhibited XRD peaks either due to α- or β-Si_3N_4 material confirming the formation of β-SiAlON phase upon reaction sintering. The increase of β-SiAlON phase with the increase of the *z* value (i.e. with Al_2O_3 and AlN concentration) could also be attributed to the increased diffusion of ions or to the enhanced reaction of precursor materials in relatively larger amount of tri-oxide eutectic melt (i.e. liquid-phase) formed due to the reactions between Al_2O_3 and Y_2O_3 and/or SiO_2 at <1600°C [73]. The SiO_2 is a product of the surface oxidation of Si_3N_4, which is difficult to avoid. The amount of Si_3N_4 and Al_2O_3 required for the formation of β-$Si_5Al_1O_1N_7$ (Z1Y7) are about 80.57% and 11.71%, respective-

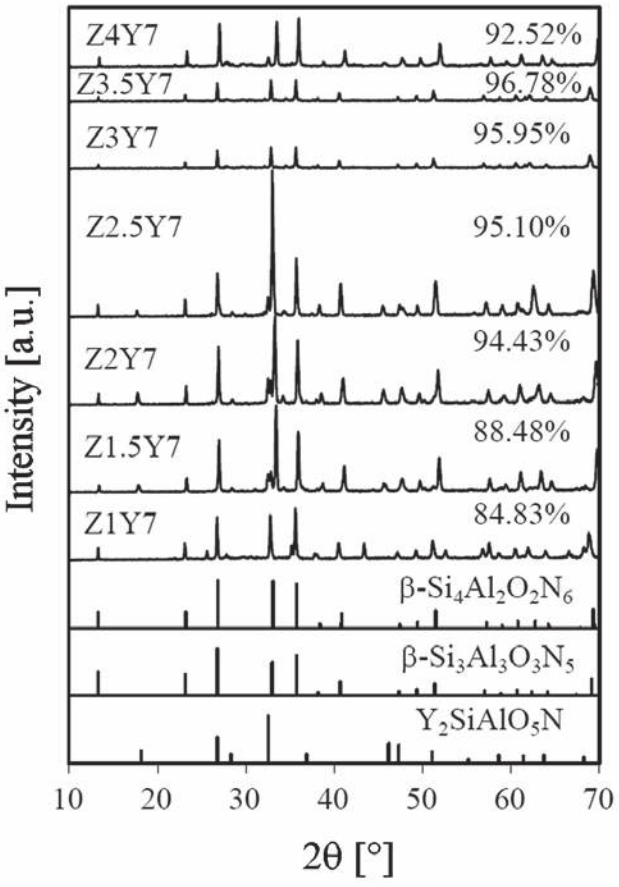

Figure 3. XRD patterns of various β-$Si_{6-z}Al_zO_zN_{8-z}$ (*z* = 1-4) ceramics sintered with 7 wt.% Y_2O_3 at 1675°C for 4 h (Y_2SiAlO_5N - ICDD: 00-048-1627; β-$Si_3Al_3O_3N_5$ - ICDD: 00-036-1333; β-$Si_4Al_2O_2N_6$ - ICDD: 00-048-1616)

Table 4. GD of pressed compacts and BD, AP and WA of β-$Si_{6-z}Al_zO_zN_{8-z}$ (*z* = 1-4) ceramics sintered at 1675°C for 4 h with 3 and 5 wt.% Y_2O_3 [24]†

Composition	Materials sintered with 3 wt.% Y_2O_3					Materials sintered with 5 wt.% Y_2O_3				
	Code‡	GD [kg/m³]	BD [kg/m³]	AP [%]	WA [%]	Code‡	GD [kg/m³]	BD [kg/m³]	AP [%]	WA [%]
Si_5AlON_7 (Z1)	Z1Y3	2050	2640	15.31	5.80	Z1Y5	1830	2750	9.34	3.39
$Si_{4.5}Al_{1.5}O_{1.5}N_{6.5}$ (Z1.5)	Z1.5Y3	1850	2780	8.70	3.13	Z1.5Y5	1840	2850	6.33	2.22
$Si_4Al_2O_2N_6$ (Z2)	Z2Y3	1880	2800	7.01	0.02	Z2Y5	1860	2930	3.85	1.31
$Si_{3.5}Al_{2.5}O_{2.5}N_{5.5}$ (Z2.5)	Z2.5Y3	2000	2750	5.23	1.37	Z2.5Y5	1920	3010	3.01	1.40
$Si_3Al_3O_3N_5$ (Z3)	Z3Y3	2020	2950	4.42	1.50	Z3Y5	1960	3000	3.00	1.55
$Si_{2.5}Al_{3.5}O_{3.5}N_{4.5}$ (Z3.5)	Z3.5Y3	1930	3100	1.86	0.60	Z3.5Y5	1960	2890	2.08	0.71
$Si_2Al_4O_4N_4$ (Z4)	Z4Y3	1970	3110	2.48	0.80	Z4Y5	1950	3020	6.15	2.03

† Values are derrived as mentioned in the experimental section. GD-green density; BD-bulk density; AP-apparent porosity; WA-water absorption capacity.

‡ In the sample codes, numbers 1, 1.5, 2, 2.5, 3, 3.5 & 4 represent the z value in β-$Si_{6-z}Al_zO_zN_{8-z}$ composition and the numbers 3 and 5 represent the sintering aid (Y_2O_3) concentration in the composites.

ly, whereas, for $Si_2Al_4O_4N_4$ (Z4Y7), they are only about ~31.92% and 46.4%. Since, the ionic character of Al_2O_3 (63.21%) is higher than that of Si_3N_4 (30.23%), the precursor mixture with higher alumina content is expected to react more readily leading to the improved formation of β-SiAlON phase [73]. Furthermore, as ionic materials possess relatively weaker bonds, they would break up easily during reaction sintering leading to a faster diffusion of ions to form improved β-SiAlON content [73].

Table 4 presents the green density (GD) of consolidates formed in CDPP process, and bulk density (BD), apparent porosity (AP) and water absorption (WA) capacity of various β-SiAlON ceramics sintered at 1675°C for 4 h with 3 and 5 wt.% Y_2O_3. The values of GD, BD, AP, and WA together with the percentage of the ionic character, hardness, fracture toughness, coefficient of thermal expansion (CTE), content of XRD phase and dielectric constant of β-SiAlON ceramics sintered with 7 wt.% Y_2O_3 under identical sintering conditions are presented in Table 5. At the foot notes of these tables, the given sample codes are explained. It can be seen that, in general, the GD and BD values of the consolidates increased with the increase of z value as well as Y_2O_3 in the composition, and as a consequence, their AP and WA capacities values decreased. The increase of GD with the increase of z value could be attributed to the increased content of high density Al_2O_3 (3970 kg/m^3) in the compacted consolidate. After sintering for 4 h at 1675°C, only Z3.5Y3, Z4Y3, Z2Y7, Z2.5Y7 and Z3Y7 materials exhibited BD values of >3020 kg/m^3 (Tables 4 and 5). Recently, β-SiAlON with a BD of 3020 kg/m^3 was found to be suitable for certain radome applications [2–5]. When sintered at 1700°C for 4 h with 7 wt.% Y_2O_3 all compositions except Z1Y7 and Z4Y7, exhibited BD values higher than 3020 kg/m^3, and AP and WA capacity values lower than 1 and 0.5%, respectively. The reason for not as good sintering of the extreme compositions of the β-SiAlON (i.e., Z1Y7 and Z4Y7) even with 7 wt.% Y_2O_3 could be mainly attributed to the non-uniform distribution of minor components of precursor mixtures in the pressed compact due to their smaller contents [2–5]. A close look at the data of Tables 4 and 5 reveals two important points. The first - as the z value increases, the sinterability of β-SiAlON ceramics in general increases irrespective of the Y_2O_3 concentration. In the case of materials with $z \geq 3.5$, even 3 wt.% Y_2O_3 is sufficient to densify the material to 3020 kg/m^3 (i.e., >98% of theoretical density) at 1675°C for 4 h. The second - all samples, besides the ones with extreme compositions (i.e. β-Si_5AlON_7 and β-$Si_2Al_4O_4N_4$) in the wide range of β-SiAlON solid solutions [2–5], underwent reasonably acceptable densification upon sintering at 1675°C for 4 h in the presence 7 wt.% Y_2O_3. The higher densification behaviour of β-SiAlON ceramics with higher alumina content could be explained based by their higher percentage of ionic character. The percentage of ionic character (IC) of Si_3N_4, Al_2O_3, AlN and Y_2O_3 were estimated to be 30.23%, 63.21%, 43.02% and 73.33%, respectively, as per the relation: ($IC = 1 - \exp[-1/4(X_A - X_B)^2]$, where X_A and X_B are the electronegativity of the bonding atoms). The Pauling's electronegativity (EN) data of Si - 1.8; Al - 1.5; Y - 1.2; O - 3.5; N - 3.0 was used in these calculations [74,75]. The percentage of ionic character data of the raw materials was used to calculate the percentage of ionic character of various β-SiAlON ceramics prepared in this study based on the rule of mixture of their values as presented in Table 5. As can be noted from this table, the percentage of ionic character is increased with the increase of alumina concentration. The presence of higher ionic character could be responsible for noted BD values more than 3020 kg/m^3 for $Si_{2.5}Al_{3.5}O_{3.5}N_{4.5}$ (49.981%) and $Si_2Al_4O_4N_4$ (52.11%) ceramics upon sintering at

Table 5. Physico-mechanical properties of β-SiAlON ceramics sintered at 1675°C for 4 h [24]†

Sample code‡	GD [kg/m^3]	BD [kg/m^3]	AP [%]	WA [%]	Ionic character [%]	CTE (×10^{-6}/°C) (30-700°C)	Hardness [kg/mm^2]	Fracture toughness [MPa.m$^{1/2}$]	β-SiAlON phase [%]	Dielectric constant at 17 GHz frequency
Z1Y7	1830	2830	7.09	2.50	38.903	-	-	-	84.83	5.67
Z1.5Y7	1880	2960	4.99	1.69	40.973	3.532	-	-	88.48	6.32
Z2Y7	1870	3070	0.01	0.00	43.363	3.628	1317±5	3.30±0.4	94.43	7.206
Z2.5Y7	1960	3050	0.04	0.01	44.958	3.778	1252±4	2.75±0.2	95.10	7.35
Z3Y7	1960	3020	0.01	0.01	47.788	3.827	1276±4	2.64±0.2	94.95	6.82
Z3.5Y7	1980	2990	0.31	0.10	49.981	4.405	1281±5	2.78±0.3	96.78	6.89
Z4Y7	1940	2920	4.72	1.61	52.110	4.657	1278±3	4.34±0.4	92.52	7.67

† Values are derrived as mentioned in the experimental section; CTE-coefficient of thermal expansion; GD-green density; BD-bulk density; AP-apparent porosity; WA-water absorption capacity

‡ In the sample codes, numbers 1, 1.5, 2, 2.5, 3, 3.5 & 4 represent the z value in β-$Si_{6-z}Al_zO_zN_{8-z}$ composition and the number 7 represents the sintering aid (Y_2O_3) concentration in the composites.

1675ºC for 4 h even with 3 wt.% Y_2O_3 employed. It is also a known fact that materials with higher percentage of ionic character (i.e. ≥50%) undergo higher densification in comparison to those having lower percentage of ionic character (i.e. <50%) such as Si_3N_4, SiC, B_4C, etc. [73–75].

It can also be seen from Table 5 that all the materials exhibited reasonably high hardness (1252 to 1317 kg/mm^2) and fracture toughness (2.64 to 4.34 MPa m$^{1/2}$) values. These fracture toughness values are well comparable with those values reported in the literature for similar ceramics [76]. The hardness of the material decreased and its fracture toughness increased with the increase of z value, i.e. with increase of aluminium and oxygen content in the β-SiAlON network. The three-point bend strength of $Si_4Al_2O_2N_6$ (Z2Y7) was found to be ~226 MPa after sintering at 1675°C for 4 h. A value of ~260 MPa was reported for the same composition made by an aqueous gelcasting route by ORNL, USA [2–5]. It has also been reported that with the increase of alumina content, the amount of liquid phase to be formed by reactions between Al_2O_3 and SiO_2 at an eutectic temperature of 1587°C is also increased [75]. It is a known fact that the liquid phase favours the formation of elongated grains during sintering operation and that presence in the case of high z materials could be responsible for the observed higher fracture toughness values.

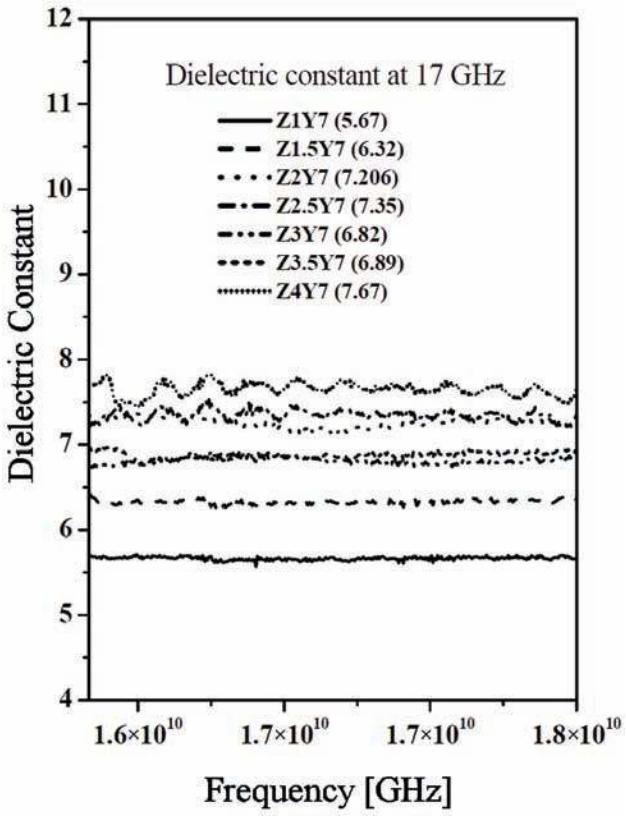

Figure 4. Influence of chemical composition on dielectric constant of β-$Si_{6-z}Al_zO_zN_{8-z}$ (z = 1-4) ceramics sintered with 7 wt.% Y_2O_3 at 1675°C for 4 h [24]

The SEM study of β-$Si_{6-z}Al_zO_zN_{8-z}$ (z = 1, 1.5, 2, 2.5, 3, 3.5 and 4) ceramics sintered with 7 wt.% Y_2O_3 at 1675°C for 4 h revealed the presence of only elongated (2 to 10 μm in length and 2 to 3 μm in diameter) grains in ceramics with z = 2.5, 3, 3.5 and 4, whereas, the combination of elongated and equi-axed grains (about <5 μm in diameter) in those with z = 1, 1.5 and 2 [24]. This study further revealed that there is a gradual decrease of porosity percentage in the micrographs with the increase of z value in β-$Si_{6-z}Al_zO_zN_{8-z}$. The ceramics with z = ≤2.5 had considerable amount of glassy phase. These results are also inline to the information reported in the literature [2–5].

Dielectric constants of β-SiAlON ceramics (Z1Y7-Z4Y7, Table 5) sintered at 1675°C for 4 h are recorded in the frequency range of 16 to 18 GHz and the corresponding profiles are presented in Fig. 4. It can be seen that all the materials exhibited reasonably stable and low dielectric constant values. At 17 GHz, the dielectric constant of these materials varied between 5.67 and 7.67. It is known that the overall dielectric constant of a material originates from different polarisation mechanisms such as electronic (P_e), ionic (P_i), orientation (P_o), space charge (P_{sc}), etc., and it is also highly influenced by the material composition, frequency of applied field, temperature of the dielectric, humidity, crystal structure, etc., and by other external factors including porosity [77,78]. Further, the polarisations from P_e and P_i are mostly composition dependent, instantaneous, or nearly frequency independent for most dielectrics and only marginally affected by temperature, and on the hand the P_o is both frequency (time) and temperature dependent. This polarisation is slower than the ionic polarisation. The P_{sc} is associated with ion migration, presence of grain boundary or inhomogeneous phases in the dielectric and is the slowest process [77]. Since, in the present case, the applied frequency is varied through 16 to 18 GHz at ambient conditions, the operative polarisations are mainly electronic, and ionic [77,78]. As there is no apparent correlation between the porosity and dielectric constant data of the β-SiAON ceramics (Table 5), the observed differences in the dielectric constant values could be related to the differences mainly in the chemical compositions. For example, materials with z = 3, 3.5 and 4 have apparent porosity (AP) values of 0.01, 0.31 and 4.72%, respectively, whereas, their corresponding dielectric constant values are 6.82, 6.89 and 7.67, respectively. If the porosity had a strong influence on the measured dielectric constant of these materials, there should have been a decreasing trend in the dielectric constant values with the increase of porosity. However, such trend is absent in the present case (Table 5). Thus, it can be inferred from these results that the presence of negligible amount of porosity could be responsible for not finding any correlation between AP and dielectric constant values of these materials. The die-

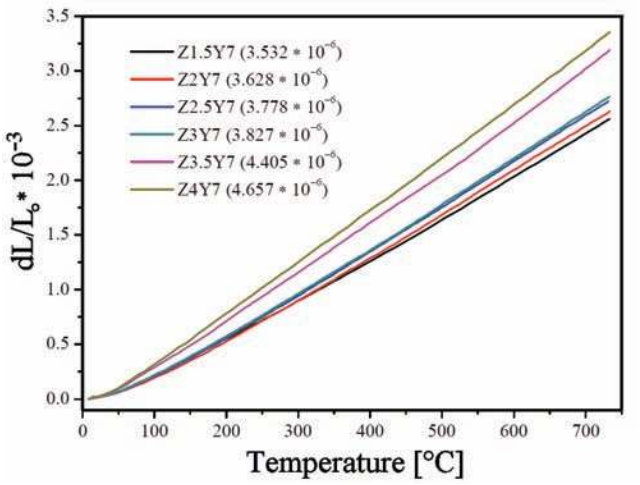

Figure 5. CTE profiles of various β-SiAlONs sintered with 7 wt.% Y_2O_3 at 1675°C for 4 h [24]

lectric constant reported for a gelcast β-$Si_4Al_2O_4N_6$ varied between 6.84 and 7.46 [2–5]. Thus, the observed dielectric constants of these materials are comparable with those reported in the literature.

The recorded CTE profiles of various β-SiAlON ceramics sintered at 1675°C for 4 h with 7 wt.% Y_2O_3 are presented in Fig. 5 between 30 and 700°C temperatures. A gelcast β-SiAlON having a nominal composition of $Si_4Al_2O_2N_6$ exhibited a value of 4.1×10^{-6}/°C between 25 and 1000°C [2–5]. It can be seen that as the *z* value increased from 1.5 to 4, the CTE value increased gradually from 3.532 to 4.657×10^{-6}/°C. The increase of CTE with the increase of *z* value, i.e. with the alumina content in the SiAlON matrix, could be related to the increase in the percentage of ionic character of these materials. As the ionic character increases the strength of the bond existing between the atoms becomes weak thereby the inter-atomic distance increases at high temperatures leading to the higher CTE values. The CTE values observed in the present study are also comparable with reported results [2–5].

This study clearly suggests that among the different compositions sintered with different amounts of Y_2O_3, the β-$Si_4Al_2O_2N_6$ sintered with 7 wt.% Y_2O_3 (i.e. Z2Y7, Table 5) at 1675°C for 4 h exhibits the best combination of properties including BD of ~3067 kg/m^3, AP of ~0.012%, WA capacity of ~0.004%, XRD phase of ~94.43%, ~1317 kg/mm^2, fracture toughness of ~3.30 MPa.m$^{1/2}$, 3-point bend strength of ~226 MPa, CTE of 3.628×10^{-6}/°C between 30–700°C, and a dielectric constant of ~7.206 at 17 GHz [24].

3.2 Characteristics of surface passivated AlN powder

The surface of raw AlN powder is usually covered with a process-dependant alumina (i.e. θ- and γ-Al_2O_3) and/or a hydrated alumina layer (γ-AlOOH and $Al(OH)_3$) [28,29]. Such layers are further developed during storage because of poor chemical stability against oxidation and hydrolysis. These surface hydroxyl groups play a vital role in the formation of a protective layer against hydrolysis on the surface of AlN powder when treated with H_3PO_4 and $Al(H_2PO_4)_3$. The reaction of AlN surface with H_3PO_4 could be expressed as: $Al(OH)_3 + H_3PO_4 + n[Al(H_2PO_4)_3] \rightarrow (n+1)\ Al(H_2PO_4)_3 + 3H_2O$ [28,29]. In fact, the reaction occurs only between $Al(OH)_3$ and H_3PO_4, and the $Al(H_2PO_4)_3$ is expected to perform only the seeding action as $Al(OH)_3$ ultimately converts into $Al(H_2PO_4)_3$ after reacting with H_3PO_4 under the mild reaction conditions employed. It has been reported that ~1.1 mg $H_2PO_4^-$ is required to form a continuous single lamella of uni-molecular monolayer of phosphate on the square meter surface of AlN [28,29]. However, in the present case in order to ensure the coating of all the particles, ~5.0 mg $H_2PO_4^-$ (in the form of H_3PO_4) and ~3.70 mg (in the form of $Al(H_2PO_4)_3$) per square meter of AlN was taken. All in all, an excess of ~7.0 mg $H_2PO_4^-$ ions per square meter of AlN was available during reaction, which is expected to ensure the coating of all powder particles [31,32]. The excess/un-reacted phosphate ions were removed from the treated powder (T-AlN) surface by washing with absolute ethanol. The T-AlN was found to be quite stable against hydrolysis in water for ~72 h, and in an open-air atmosphere for ~3 months. A schematic representation of the monolayer coverage of $H_2PO_4^-$ on the surface of AlN particle is shown in Fig. 6.

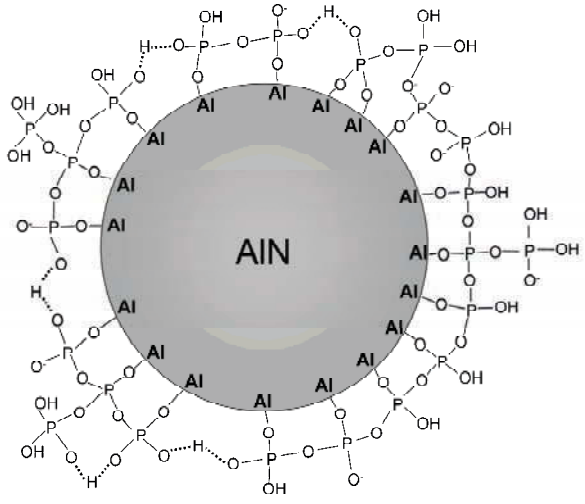

Figure 6. Schematic representation of the phosphate layer chemisorbed onto the surface of an AlN powder particle [31]

The XRD patterns of the as-purchased A-AlN (A-AlN-72 h) and treated T-AlN (T-AlN-72 h) powders after suspending in water for 72 h are presented in Fig. 7. The A-AlN-72 h powder is mainly $Al(OH)_3$ (ICDD File No.: 00-020-0011) together with some minor portion of un-reacted AlN. On the other hand, the T-AlN-72 h powder is completely AlN (ICDD File No.: 00-025-

1133) indicating that the surface treated AlN powder is quite stable in water. SEM micrograph and EDAX spectra of T-AlN-72h are presented in Fig. 8a,c and of A-AlN-72h in Fig. 8b,d, respectively. The A-AlN powder (having average particle size of ~7.62 μm) converted into relatively large sized agglomerates (>50 μm) after suspending in water for 72 h. A close look at its micrograph (Fig. 8b) gives an impression that the fine A-AlN-72h particles are fused together to form continuous cement like network after suspending in water for 72 h. EDAX results reveal that T-AlN-72h (Fig. 8c) consists nitrogen as a major element, whereas, A-AlN-72 h (Fig. 8d) consists Al and O as major constituents. The XRD, SEM and EDAX study confirmed that a major part of the as-purchased AlN (A-AlN) was converted into $Al(OH)_3$ upon suspending in water for 72 h, whereas the T-AlN is quite stable after being suspended in water for 3 days [31,32].

3.3 Properties of aqueous processed β-$Si_4Al_2O_2N_6$ ceramics

The component making capability of GC, HAS and GCHAS processes from aqueous β-$Si_4Al_2O_2N_6$ precursor mixtures' slurries could be seen from Table 6 [19,58]. This table also shows the medium employed for each slurry preparation, the conditions of green radomes/crucibles/tubes and rectangular bars formed in each process, the amount of time taken for each process and the solids loading and absolute viscosity of the slurry. Many details pertaining to these slurries' preparations are given at the footnotes of this table. The precursor mixtures compositions employed for preparing each of suspensions are presented in Table 3 [19]. Nor-

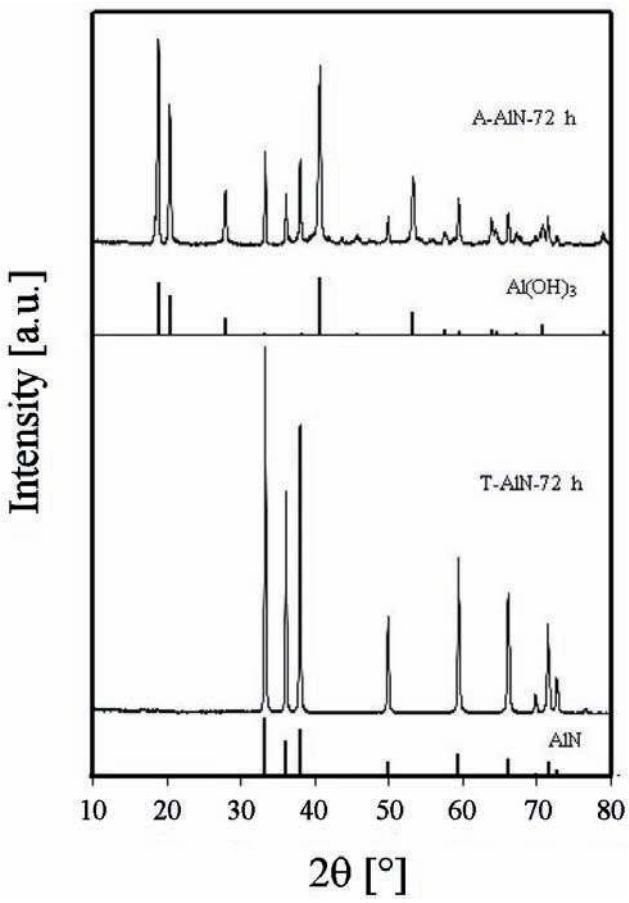

Figure 7. XRD patterns of different AlN powders (AlN - ICDD: 00-025-1133; and $Al(OH)_3$ - ICDD: 00-020-0011) [19]

Table 6. Slurry characteristics and condition of green radomes, crucibles, tubes and rectangular bars consolidated from aqueous particulate slurries containing 48-50 vol.% β-$Si_4Al_2O_2N_6$ precursors mixtures by following HAS (HAS-5 to HAS-15), GC (GC-SSC9 and GC) and GCHAS (GCHAS-2 to GCHAS-10) routes [19]

Sample code	Solids loading [vol.%]	Viscosity [mPa·s]	Slurry medium[†]	Gelation conditions	Condition of the green rectangular bar	Condition of green crucible/tube/ radome
GC-SSC9	48	288.5	CPM / NCPM	3 h at 30ºC	Acceptable	Acceptable
HAS-5	50	299.6	Water	3 h at 30ºC followed by 6 h at 60ºC	Acceptable	Not acceptable
HAS-10	50	514.5	Water	3 h at 30ºC followed by 6 h at 60ºC	Not acceptable	Not acceptable
HAS-15	50	823.0	Water	3 h at 30ºC followed by 6 h at 60ºC	Not acceptable	Not acceptable
GC[‡]	48	678.0	NCPM	3 h at 30ºC followed by 2 h at 60ºC	Acceptable	Acceptable
GC[♀]	50	246.0	NCPM	3 h at 30ºC followed by 6 h at 60ºC	Acceptable	Not acceptable
GCHAS-2	50	248.4	CPM / NCPM	3 h at 30ºC followed by 2 h at 60ºC	Acceptable	Acceptable
GCHAS-5	50	276.8	CPM / NCPM	20 min at 30ºC	Acceptable	Acceptable
GCHAS-7	50	512.7	CPM / NCPM	15 min at 30ºC	Acceptable	Acceptable
GCHAS-10	50	717.8	CPM / NCPM	15 min at 30ºC	Not acceptable	Not acceptable

[a] Details are given in the experimental section; [‡] Involved treated AlN powder without washing.
[♀] Involved treated AlN (T-AlN) powder after washing with absolute ethanol for 48 h.
[†] NCPM stands for non-conventional premix solution formed by the dissolution of 20 wt.% MAM, MBAM, and NVP in 3:1:3 ratio in distilled water, CPM stands for conventional premix solution formed by the dissolution of 17 wt.% MAM and MBAM in 3:1 ratio in distilled water.

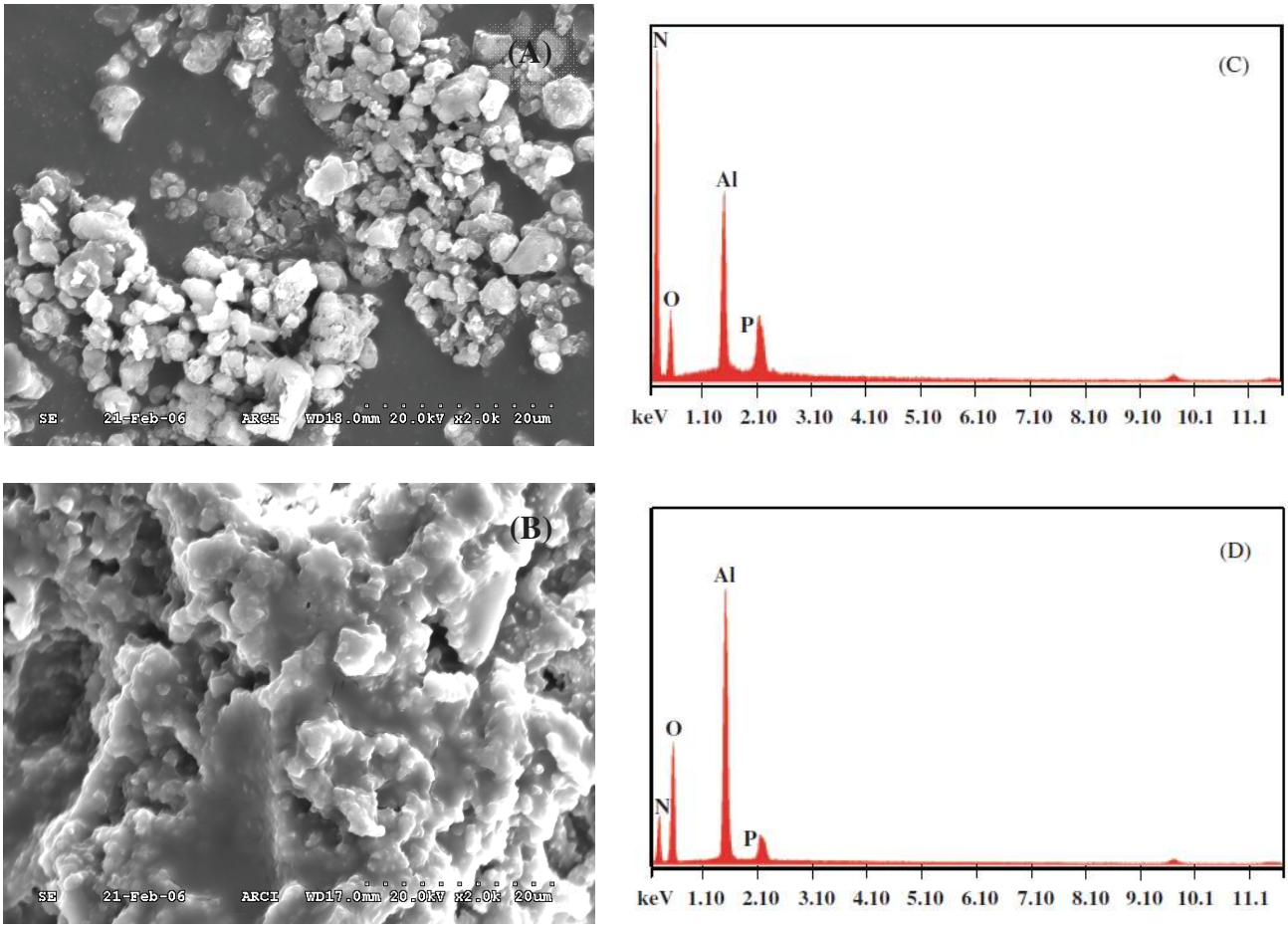

Figure 8. SEM micrograph and EDAX spectra of T-AlN-72h (a & b), and A-AlN-72h (c & d), respectively [19]

mally, to obtain a defect free consolidate by any colloidal processing route, the viscosity of the slurry should be kept ≤300 mPa·s [22]. Although aqueous gelcasting (GC) is known for providing exceptionally high flexural strength to the green bodies, fabrication of certain structures such as radomes, crucibles, tubes, etc., following this route is relatively difficult. This is due to the fact that the mandrel needs to be removed from the mould prior to the cast part gets completely gelled/dried, which causes breaking of the part within the mould due to excess shrinkage of the part when the solids loading in the slurry is not optimum. The minimum solids loading required for making defect free radomes, crucibles and tubes out of β-$Si_4Al_2O_2N_6$ precursor mixtures' slurries was found to be 48 vol.% [19,58]. When the solids loading was less than this ratio, the slurry took more time to get gelled to the required extent. Furthermore, in this case, the gelled parts were always found to be cracked as the mandrel could not allow the part to shrink to get the enough strength.

The slurries consisting of precursor mixtures of GC-SSC9, HAS-5, GCHAS-2, GCHAS-5, and GC with partially washed T-AlN (Table 6) exhibited absolute viscosity values <300 mPa·s. The green parts cast out of all of these slurries had shape integrity upon drying, and they exhibited green densities >50% of the theoretical density (TD) upon drying. The HAS-5 slurry exhibited a viscosity <300 mPa·s, which was responsible for forming acceptable quality rectangular bars (Table 6). Although the rectangular bars formed out of HAS-10 and HAS-15 were found to be very strong, they had considerable amount of porosity in them. Further, none of the HAS suspensions led to the formation of defect free radome/crucible/tube structures.

In the case of GC slurries (Table 6), they needed ~10 µL of APS (initiator) and ~10 µL of TEMED (catalyst) per gram of slurry to convert into gel. Furthermore, this slurry could not be converted into gel under ambient conditions but converted at ~55–60°C in an electrically heated oven. Furthermore, in this case, the surface passivated AlN powder against hydrolysis (T-AlN) had a strong influence on the slurry viscosity and on its gelation behaviour. When T-AlN was not washed thoroughly with absolute ethanol in order to remove the un-reacted excess phosphate ions from its surface completely, an improved gelation of slurry was noted in comparison to the one involved the fully washed T-AlN powder [19]. These results suggest that prolonged washing of T-AlN with absolute ethanol creates certain specific sites, which preferentially interact with APS free radicals during polymerisation of organic gelcast monomers, i.e. MAM, MBAM and NVP. In this case, the number of

APS free radicals available for initiating the polymerization reaction of organic monomers would be lowered, hence a delayed or weak gelation. However, when the as treated T-AlN was employed without much washing, the slurry underwent relatively faster gelation though it has restricted the maximum achievable solids loading in the slurry to only 48 vol.% only. In addition to this, this slurry (GC) also consumed about 2 to 6 h time at 55–60°C to undergo complete gelation. The temperature induced gelation is not recommended for SiAlON ceramics as there will be considerable number of gas releasing reactions between Si_3N_4 and APS/TEMED that creates a lot of porosity in the green body. Nevertheless, GC could not lead to any radome or crucible shape even upon temperature induced gelation (Table 6) [19].

On the other hand, the slurries, GCHAS-2 to GCHAS-7 exhibited faster gelling behaviour upon introducing APS and TEMED even at the ratio of 2 and 4 μL per gram of slurry, respectively, under simple ambient conditions (Table 6). The time consumed in setting of GCHAS-5 at ambient conditions was found to be <20 min. Nevertheless, this time could always be delayed by adding relatively smaller amounts of APS and TEMED or by cooling the slurry close to ~5°C in a refrigerator prior to introducing APS and TEMED [22]. The improved gelation in the case of GCHAS process could be ascribed to the synergy of HAS and GC processes. The gelled parts of GCHAS-5 and GCHAS-7 slurries were found to be like a strong rubber until they were completely dried. These parts were also found to be relatively stronger than those formed out of GC and HAS slurries. Thus, these results clearly reveal that the GCHAS is a more promising technique for making thin wall β-$Si_4Al_2O_2N_6$ radomes, crucibles, tubes, etc., with near-net shape in comparison to HAS and GC processes.

Table 7 reveals the values of bulk density (BD), apparent porosity (AP), water absorption capacity (WA), total linear shrinkage (LS), hardness, fracture toughness and β-SiAlON phase contents of β-$Si_4Al_2O_2N_6$ ceramics consolidated from slurries containing HAS-5, GC and GCHAS-5 precursor mixtures (Table 3) and sintered for 4 h at 1675°C, and of β-$Si_4Al_2O_2N_6$-9 wt.% SiO_2 ceramic composite consolidated from a slurry having GC-SSC9 precursor mixture and sintered for 4 h at 1750°C along with the green density (GD) values of these consolidates [19]. It can be seen that both β-$Si_4Al_2O_2N_4$ and

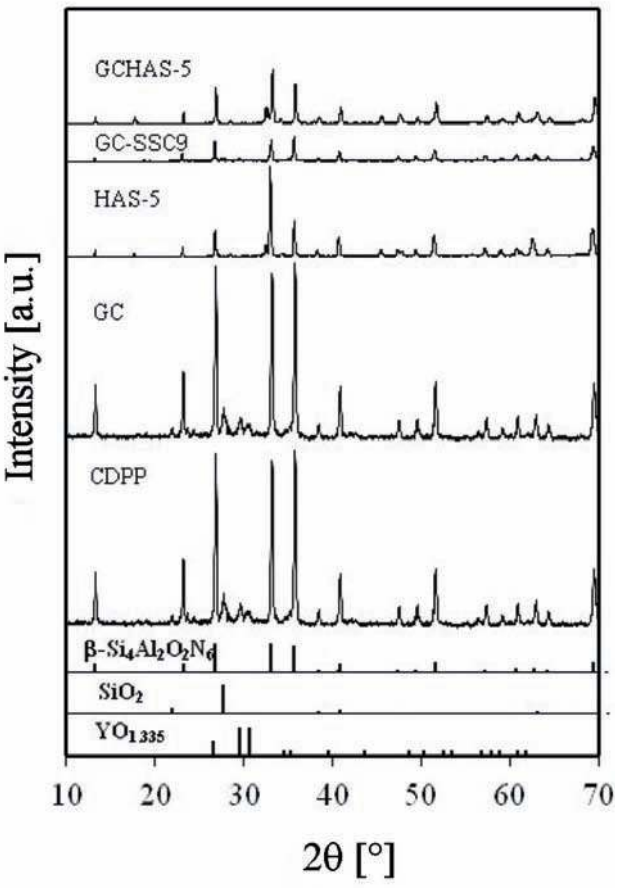

Figure 9. XRD patterns of β-$Si_4Al_2O_2N_6$ ceramics formed from (a) HAS-5, (b) GC and (c) GCHAS-5 precursor mixtures and of β-$Si_4Al_2O_2N_6$-9 wt.% SiO_2 ceramic composite formed from (d) GC-SSC9 precursor mixture, sintered at 1675°C and 1750°C, respectively ($YO_{1.335}$ - ICDD: 00-039-1065; SiO_2 - ICDD: 01-085-0462; β-$Si_4Al_2O_2N_6$ - ICDD: 00-48-1616)

Table 7. Properties of β-$Si_4Al_2O_2N_6$ (HAS-5, GC and GCHAS-5) ceramics and β -$Si_4Al_2O_2N_6$-9 wt.% SiO_2 ceramic composites (GC-SSC9) sintered at 1675°C and 1750°C for 4 h, respectively [19]

Sample codes♀	GD [kg/m³]	BD [kg/m³]	AP [%]	WA [%]	Total linear shrinkage [%]	β-SiAlON phase [%]	Hardness [kg/mm²]	Fracture toughness [MPa.m$^{1/2}$]
GC-SSC9‡	1750	3130	1.0	1.0	~17	~90	1356±8	3.42±0.3
HAS-5	1730	3120	0.47	0.16	~14	~94	1571±11	3.42±0.2
GC	1860	3070	0.13	0.04	<16	~93	1423±4	3.95±0.3
GCHAS-5	1960	3150	0.01	0.01	<16	~94	1495±7	3.56±0.2

♀ SSC9 stands for SiAlON-SiO_2 ceramic composite having 9 wt.% SiO_2; GC stands for aqueous gelcasting; HAS stands for hydrolysis assisted solidification; GCHAS stands for hydrolysis induced aqueous gelcasting; 0 and 5 indicates A-AlN content in the precursor mixtures; GD-green density; BD-bulk density; AP-apparent porosity; WA-water absorption capacity

‡ Made using slurry containing 48 vol.% precursor solids, and the rest are made used slurries containing 50 vol.% precursor solids loading.

β-$Si_4Al_2O_2N_6$-9 wt.% SiO_2 ceramics exhibited BD values >3020 kg/m^3. The small difference seen in the GD values seems to have little effect on their densification behaviour upon sintering as all these sintered ceramics exhibited almost similar BD values (i.e., 3070 to 3150 kg/m^3). The total LS associated with ceramics made from slurries containing HAS-5, GC and GCHAS-5 precursor mixtures were found to be less than 17%, which is well within the acceptable range for making complex-shaped parts [2,22]. The higher sintering behaviour of β-$Si_4Al_2O_2N_6$ precursor mixtures used in this study could be attributed not only to the use of higher sintering temperature (1675°C for 4 h) and the Y_2O_3 content (7 wt.%), but also to the involvement of high purity powders having small average particle sizes. The reason for requiring higher sintering temperature (i.e. at 1750°C for 4 h) for β-$Si_4Al_2O_2N_6$-9 wt.% SiO_2 ceramic composite in comparison to β-$Si_4Al_2O_2N_6$ ceramics could be attributed to the excess 9.0 wt.% SiO_2 present in the former material. The SiO_2 is known for restricting grain diffusion to some extent by forming a high viscous liquid during sintering thereby demanding the higher sintering temperatures [18,23,34–37,73].

XRD patterns of various β-$Si_4Al_2O_2N_4$ ceramics sintered for 4 h at 1675°C, and of β-$Si_4Al_2O_2N_4$-9 wt.% SiO_2 ceramic composite sintered for 4 h at 1750°C are presented in Fig. 9 [19]. It can be seen that all the materials are fully crystalline and are mainly (>90%) β-SiAlON ceramics (ICDD File No.: 00-48-1616) phase. The formation of Y_2SiAlO_5N (ICDD File No.: 00-048-1627) is expected in these materials due to the reactions between SiO_2, Al_2O_3 and Y_2O_3 at sintering temperature; however, no characteristic peaks belonging to this phase are noticed. The probable reason for not detecting any characteristic peaks of this phase is the crystallite size of this material could be below the detection limit of XRD technique. However, some minor peaks belonging to SiO_2 (ICDD File No.: 00-085-0462) and $YO_{1.335}$ (ICDD File No.: 00-039-1065) are revealed by ceramics consolidated from CDPP and GC precursor mixtures, both of which are the starting materials for Y_2SiAlO_5N formation. These XRD results are well-comparable with those reported by Janney and others [3–5]. Although β-$Si_4Al_2O_2N_4$-9 wt.% SiO_2 ceramic composite contains ~9 wt.% free SiO_2, no characteristics XRD peaks due to this silica phase are seen [18]. It has been reported that

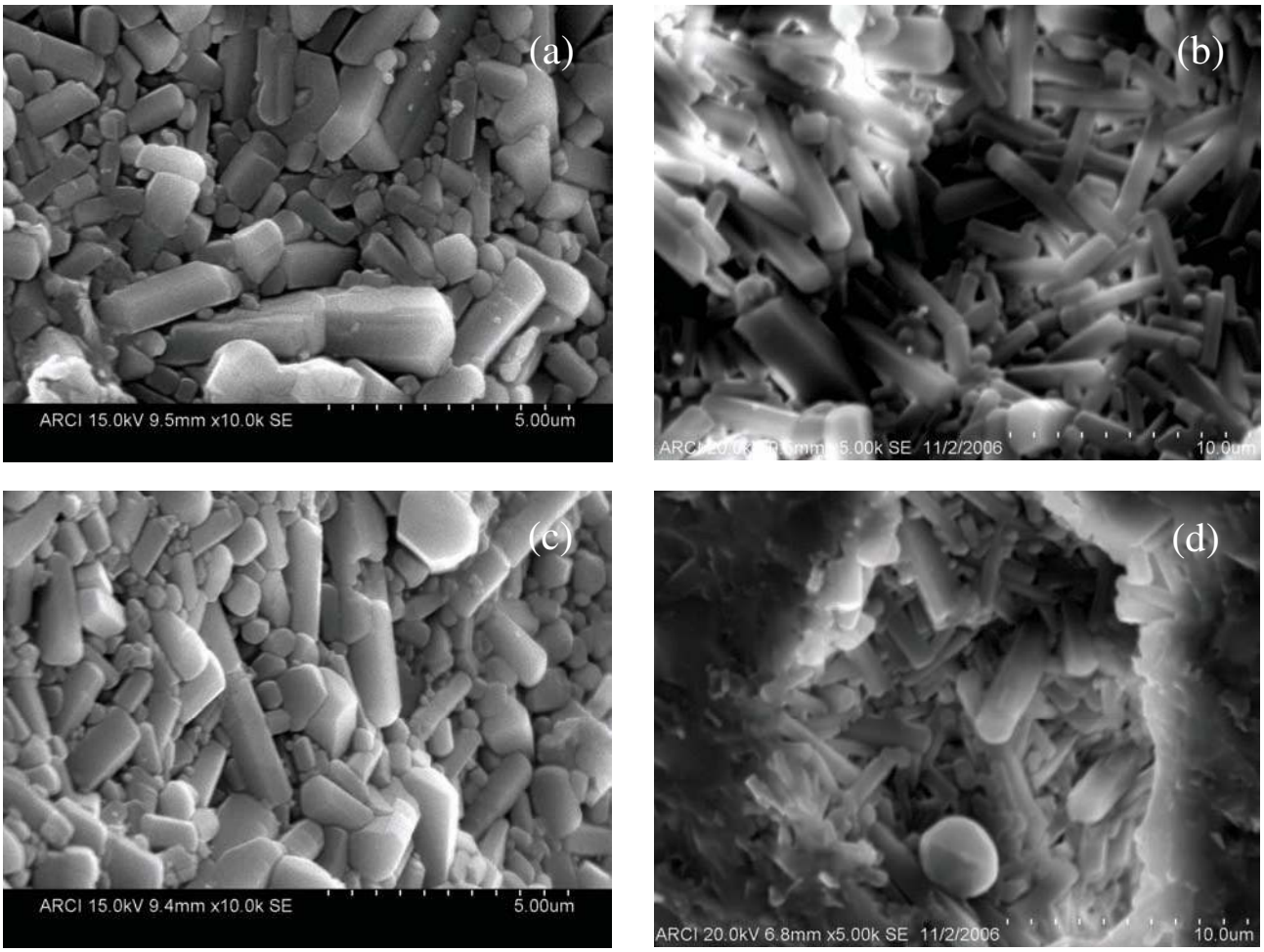

Figure 10. SEM micrographs of different types of β-$Si_4Al_2O_2N_6$ ceramics formed from (a) HAS-5, (b) GC and (c) GCHAS-5 precursor mixtures and of β-$Si_4Al_2O_2N_6$-9 wt.% SiO_2 ceramic composite formed from (d) GC-SSC9 precursor mixture, sintered at 1675°C and 1750°C, respectively[19]

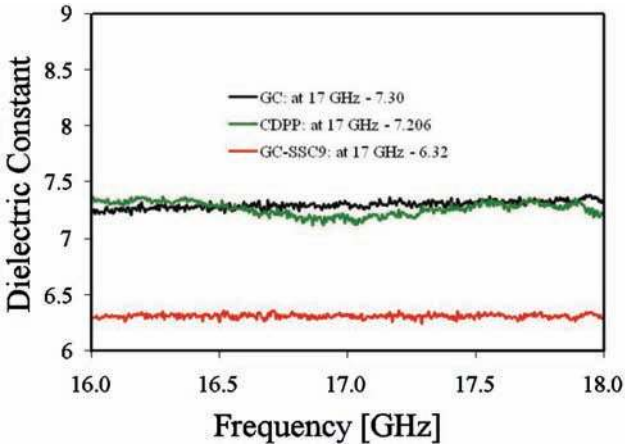

Figure 11. Dielectric constant profiles of different types of β-$Si_4Al_2O_2N_6$ ceramics formed from GC and CDPP precursor mixtures and of β-$Si_4Al_2O_2N_6$-9 wt.% SiO_2 ceramic composite formed from GC-SSC9 precursor mixture, sintered at 1675°C and 1750°C, respectively [19]

SiO_2 formed by the surface oxidation of Si_3N_4 is always in the form of amorphous phase and it reveals no characteristic XRD lines. Furthermore all these sintered materials exhibited reasonably high hardness (1317–1571 kg/mm^2) and fracture toughness (3.30–3.95 MPa.m$^{1/2}$) values (Table 7) [2].

The SEM micrographs of the colloidal processed β-$Si_4Al_2O_4N_6$ ceramics formed from HAS-5, GC and GCHAS-5 precursor mixtures at 1675ºC for 4 h, and the β-$Si_4Al_2O_2N_6$-9 wt.% SiO_2 ceramic composite formed from GC-SSC9 precursor mixture at 1750ºC for 4h are presented in Fig. 10. It can be seen that ceramics formed from HAS-5 (Fig. 10a) and GCHAS-5 (Fig. 10c) precursor mixtures consist of similar microstructures having a bimodal grains (one type being in the size range of 1–2 μm and others being ~5 μm). Interestingly, the ceramic formed from GC precursor mixture (Fig. 10b) consist almost mono-modal hexagonal grains with 1–2 μm in diameter and 5–10 μm in length. Although, the β-$Si_4Al_2O_2N_6$-9 wt.% SiO_2 ceramic composite (Fig. 10d) also consist of similar type of grains, it has some additional grains with equi-axed shape. Further, this latter material contains some pores with ~10 μm diameter in size. These SEM findings are inline to those reported for β-$Si_4Al_2O_4N_6$ ceramics formed in CDPP technique [24].

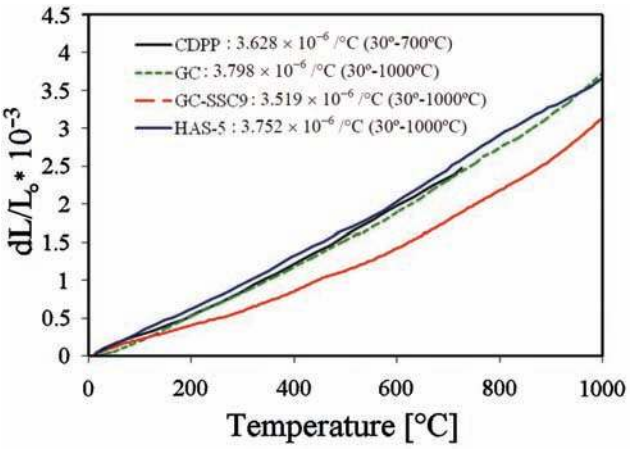

Figure 12. CTE profiles of different types of β-$Si_4Al_2O_2N_6$ ceramics formed from CDPP, GC and HAS-5 precursor mixtures and of β-$Si_4Al_2O_2N_6$-9 wt.% SiO_2 ceramic composite formed from GC-SSC9 precursor mixture, sintered at 1675°C and 1750°C, respectively [19]

Dielectric constant profiles recorded for β-$Si_4Al_2O_2N_6$ ceramics formed from GC and CDPP precursor mixtures at 1675°C for 4 h and for β-$Si_4Al_2O_2N_6$-9 wt.% SiO_2 ceramic composite formed from GC-SSC9 at 1750°C for 4 h are presented in Fig. 11 in the frequency range of 16 to 18 GHz. It can be seen that these three materials exhibited reasonably stable and low dielectric constant values. At 17 GHz, the ceramics formed from CDPP and GC precursor mixtures exhibited 7.206 and 7.30 dielectric constant values, respectively, whereas, the one formed from GC-SSC9 exhibited a value of 6.32. Since, in the present case, the applied frequency is varied from 16 to 18 GHz at ambient temperature, the operative polarisation mechanisms are mainly electronic, and ionic [75,76]. Furthermore, as these three materials exhibited very similar apparent porosity values (Table 7), the differences observed in their dielectric values do not seem to be influenced by the porosity alone but also by the chemical composition and other factors. The difference between the AP values of GC-SSC9 and others is only about 0.65% (Table 7), whereas the difference in their dielectric constant values at 17 GHz is ~13%. This data clearly indicates that the reason for difference in dielectric constant values measured for these ceramics is mainly the chemical composition as GC-SSC9 has ~ 9 wt.% excess SiO_2 in it when compared with β-$Si_4Al_2O_2N_6$ ceramics. The dielectric constant reported for a gelcast β-$Si_4Al_2O_4N_6$ varied from 6.84 to 7.46 [6–8]. Thus, the observed dielectric constant values for these synthesized materials are comparable with the reported results in the literature [6–8].

CTE profiles recorded in the range of 30–1000°C for aqueous colloidal processed β-$Si_4Al_2O_2N_6$ ceramics formed from CDPP, GC and HAS-5 precursor mixtures at 1675°C for 4 h and for β-$Si_4Al_2O_2N_6$-9 wt.% SiO_2 ceramic composite formed from GC-SSC9 precursor mixture at 1750°C for 4 h are presented in Fig. 12. The CTE values recorded for these ceramics are 3.628×10^{-6}/°C (30–700°C), 3.798×10^{-6}/°C, 3.752×10^{-6}/°C, and 3.519×10^{-6}/°C, respectively. The GC-SSC9 exhibited a relatively low CTE value (3.519×10^{-6}/°C) due to the presence of excess 9.0 wt.% SiO_2 in it, while the other materials exhibited CTE values comparable to those reported in the literature for β-$Si_4Al_2O_2N_6$ [2–5]. A gelcast β-$Si_4Al_2O_2N_6$ exhibited a value of 4.1×10^{-6}/°C between 25 and 1000°C [2]. Thus, this CTE study also reveals that β-$Si_4Al_2O_2N_6$ ceramics consolidated by CDPP, HAS, and GC routes are well comparable.

Table 8. The raw materials composition, the values of green density of pressed pellets and of various properties of reaction sintered β-$Si_4Al_2O_2N_6$ (SS), β-$Si_4Al_2O_2N_6$ densified from its powder (SSC0), ceramic composites (SSC20 to SSC80) prepared from β-$Si_4Al_2O_2N_6$ and fused silica powder mixtures, and of pure fused silica (SSC100) sintered for 3-4 h at 1500 to 1750°C under ~ 101.63 kPa N_2 pressure [21]

Ceramic composite (code) ‡	SSC0	SSC20	SSC40	SSC50	SSC60	SSC80	SSC100	SS
*β-$Si_4Al_2O_2N_6$ [wt.%]	100	80	60	50	40	20	0	α-Si_3N_4, α-Al_2O_3, AlN & Y_2O_3
*Fused silica [wt.%]	0	20	40	50	60	80	100	
Green density of pressed compact [kg/m^3]	1720	1890	1830	1660	1520	1630	1140	1770
Sintering condition employed [°C/h]	1750/3	1750/3	1750/3	1500/4	1500/4	1500/4	1675/4	1675/4
BD [kg/m^3]	3210	2840	2510	2450	2480	2260	1970	3080
AP [%]	0.01	2.47	5.44	2.15	3.29	4.72	10.72	0.19
WA [%]	0.01	0.87	2.16	0.87	1.32	2.08	5.44	0.12
LS [%]	10.15	10.29	10.68	8.77	9.99	10.69	12.41	14.0
Hardness [kg/mm^2]	1407	1347	1319	957	931	766	407	1317
Mass loss upon sintering [%]	4.86	8.03	16.69	5.57	3.35	5.03	3.90	4.46

† Values were obtained as mentioned in the experimental section.
* Starting raw materials utilized
‡ In the sample codes, SS stands for reaction sintered stoichiometric β-$Si_4Al_2O_2N_6$ prepared from the precursor mixture of α-Si_3N_4, α-Al_2O_3, AlN and Y_2O_3, and the SSC stands for ceramic composites prepared from a powder mixture of β-$Si_4Al_2O_2N_6$ and fused silica, and the numbers 0-100 represent the fused silica content in the β-$Si_4Al_2O_2N_6$ and fused silica mixtures employed to prepare these ceramic composites; BD-bulk density; AP-apparent porosity; WA-water absorption capacity

3.4 Properties of dense β-$Si_4Al_2O_2N_6$-SiO_2 ceramic composites (SSC0 to SSC100)

Table 8 lists the raw materials compositions and the values of green density (GD) of consolidates made by CDPP route, and of bulk density (BD), apparent porosity (AP), water absorption (WA) capacity, linear shrinkage (LS), hardness and percentage of mass loss (ML) occurred upon sintering of β-$Si_4Al_2O_2N_6$-SiO_2 ceramic composites at 1500–1750°C for 3–4 h. For the sake of an easy identification, different codes are also given to denote these ceramic composites. In the sample codes SS stands for the reaction sintered stoichiometric β-$Si_4Al_2O_2N_6$ ceramic, and the SSC stands for ceramic composite formed from the powder mixture of β-$Si_4Al_2O_2N_6$ and fused silica, and the numbers 0–100 represent the fused silica (SiO_2) content in the starting raw materials compositions. Prior to measuring the properties presented in Table 8, and in order to find the optimum sintering condition needed to densify each composition, all samples consolidated by CDPP route were sintered at temperatures in the range of 1500°C to 1750°C for 3–4 h, and then characterised to evaluate their shape integrity (i.e. whether the material got melted/deformed or not) and the sintered density. The characterization results of these sintered ceramic composites revealed the following observations. (i) There is a gradual increase in the value of green density of the pressed consolidate with the increase of β-$Si_4Al_2O_2N_6$ content in it (Table 8). This is due to the fact that the fused silica possesses a lower bulk density (2200 kg/m^3) than that of β-$Si_4Al_2O_2N_6$ (3100 kg/m^3). (ii) In general, the compositions having ≥50 wt.% fused silica (i.e. SSC50, SSC60 and SSC80) underwent early densification at relatively lower temperatures (at about 1500°C) in comparison to β-$Si_4Al_2O_2N_6$ rich compositions (i.e., SSC20 and SSC40), and to the pure fused silica (SSC100). The latter compositions exhibited best-sintered properties only upon sintering at 1750°C and 1675°C, respectively. The reason for early densification of fused silica rich compositions in comparison to the pure fused silica could be the formation of eutectic melts out of Y_2O_3, Al_2O_3 and SiO_2 at 1350°C during sintering. (iii) The green density values estimated based on dimensions of these pressed pellets varied in the range of 1140 kg/m^3 (for pure fused silica consolidated by CDPP route, SSC100) to 1890 kg/m^3 (for SSC20). These green density values are comparable with those reported for similar kinds of ceramics consolidated by CDPP route [2–5,21,22] (iv) The β-$Si_4Al_2O_2N_6$ densified from its same powder (i.e. SSC0) exhibited a very low apparent porosity value of <0.5% after sintering at 1750°C, whereas, all the remaining ceramic composites exhibited significantly higher apparent porosity values (up to 10.72% for SSC100) even after sintering at such high temperatures. (v) Among all the sintered samples, the reaction sintered β-$Si_4Al_2O_2N_6$ (SS) exhibited the highest degree of linear shrinkage (about 14%) followed by the pure sintered fused silica (SSC100), i.e. 12.41% [2–7,21,30]. The remaining sintered composites exhibited linear shrinkage values which are comparable to those reported for similar materials consolidated by CDPP followed by sintering [21,22]. It can also be seen from Table 8 that SSC0 to SSC40 exhibited relatively higher hardness (>1310 kg/mm^2) values in comparison to others,

which showed values in the range of 407 to 957 kg/mm^2. The presence of relatively densely packed elongated grains (discussed in the following paragraphs) in the case of β-$Si_4Al_2O_2N_6$ rich composites (i.e. SSC0 to SSC40) could be responsible for the such higher measured hardness values. Furthermore, all the SiAlON-SiO_2 ceramic composites exhibited considerable amounts of mass losses upon sintering which was to be expected for Si_3N_4 based ceramics [21,22]. Among the various sintered composites, the SSC40 exhibited the highest mass loss (16.69±0.32%) followed by SSC20 (8.03±0.21%), incidentally these two ceramic composites were sintered at highest sintering temperature employed in this study (i.e. at 1750°C for 3 h) together with SSC0 (exhibited a mass loss of 4.86±0.16%). Not only the higher sintering temperature employed could be responsible for these higher mass losses, but also the presence of certain low melting phases including Y_2SiAlO_5N and the iron based silicates formed due to iron impurities that entered during the milling of the sintered β-$Si_4Al_2O_2N_6$ extrudates. Some melted spherical grains of SSC40 had small amounts of iron (found by EDAX study, not presented here). However, on the whole the percentage of this iron based impurity grains was found to be <1 wt.%. Furthermore, this iron impurity contamination was found to be drastically reduced when the relatively harder grinding media such as Al_2O_3 and ZTA (zirconia toughened alumina) was used in place of steel balls.

XRD patterns of sintered SSCx (x = 0, 20, 40, 60, 80 and 100) samples are presented in Fig. 13. It can be seen that SSC0 is a fully crystalline material and that the major portion of it is β-SiAlON (ICDD File No.: 00-048-1616) together with some impurities like Y_2SiAlO_5N (ICDD File No: 00-048-1627) and certain other un-known phases [2,23]. The SSC20 is a mixture of β-SiAlON and Si_2N_2O (ICDD File No: 00-047-1627), whereas, the SSC40 is fully Si_2N_2O. Upon sintering, the fused silica (SSC100) was completely converted into cristobalite form. Although SSC50 was prepared from a powder mixture of 50 wt.% β-$Si_4Al_2O_2N_6$ + 50 wt.% fused silica, upon sintered it was converted into a mixture of cristobalite, β-$Si_4Al_2O_2N_6$ and Si_2N_2O. On the other hand, both SSS60 and SSC80 consists of cristobalite, β-$Si_4Al_2O_2N_6$ and Si_2N_2O with cristobalite being the major content. Interestingly, in these latter composites the starting material β-$Si_4Al_2O_2N_6$ is higher than that of Si_2N_2O. The considerable amount of viscous liquid melt formed in these two composites during sintering could not have allowed moving of the relatively isolated β-$Si_4Al_2O_2N_6$ particles with enough speed to react with and form Si_2N_2O phase [73].

As mentioned in the introduction section, certain high speed (> Mach 5) radomes see a transient temperature of about 1300°C in service. Therefore, the construction materials of these radomes should be able to withstand a temperature of at least 1300°C and also should have dielectric constants preferably less than 6 [1–15]. Among the various SiAlON-SiO_2 ceramic composites prepared in this study (as listed in Table 8), only SSC40 is expected to meet both of these requirements, i.e., the high temperature withstanding capability and the dielectric constant as it was sintered at highest sintering temperature employed in this study (1750°C) for achieving the maximum density. Furthermore, among those sintered at 1750°C, only this SSC40 contains the maximum amount of fused silica, i.e. a low dielectric constant material. Considering these facts, SSC40 was selected to consolidate into near-net shape components by following the GCHAS route, as this technique allows the fabrication of thin wall radomes with near-net shape and very high green strength (i.e. >20 MPa) [19,21,58,59–63].

The compositions of precursor mixtures utilized in the consolidation of SSC40 ceramic composites by following GCHAS route, the values of viscosity of the prepared slurries at a shear rare (γ) of 141 s^{-1}, the setting time of slurries, as well as the values of green density, percentage linear shrinkage occurred upon casting followed by drying, and the green flexural (4-point bend) strength of consolidates are presented in Table 9. In sample codes given to denote these composites, SSC40 indicates the ceramic composite formed from a

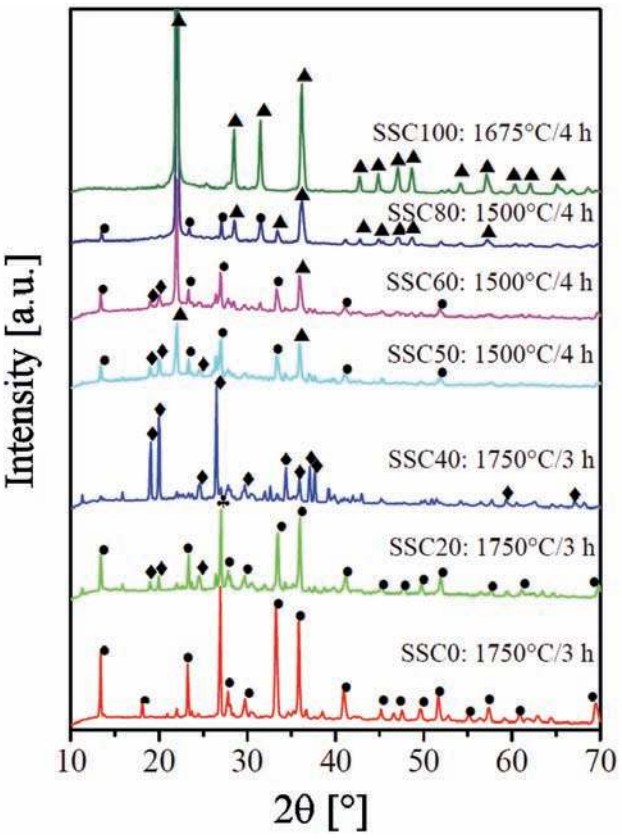

Figure 13. XRD patterns of SSCx (x = 0, 20, 40, 60, 80 and 100) ceramic composites sintered at different temperatures under N_2 atmosphere of >900 torr. (● - β-$Si_4Al_2O_2N_6$; ♦ - Si_2N_2O; ▲ - Cristobalite) [21]

Table 9. Properties of suspensions and of green bodies of 60 wt.% β-$Si_4Al_2O_2N_6$ + 40 wt.% fused silica consolidated by following GCHAS route using AlN equivalent to 1-5 wt.% Al_2O_3 [21]

Ceramic composite‡	Precursor mixture				Suspension viscosity at $\gamma = 141\ s^{-1}$ [mPa s]	Suspension setting time [min]	Green strength [MPa]	Green density [kg/m^3]	Linear shrinkage from casting to drying [%]
	β-$Si_4Al_2O_2N_6$ [%]	Fused silica [%]	A-AlN [%]	α-Al_2O_3 [wt%]*					
SSC40-1	59.51	39.67	0.80	1	503	~11	14.13±1.87	1830±0.06	2.32±0.23
SSC40-2	59.03	39.35	1.61	2	467	~10	15.32±2.17	1820±0.04	2.33±0.11
SSC40-3	58.52	39.01	2.47	3	433	~8	16.72±2.32	1820±0.05	2.33±0.32
SSC40-4	58.06	38.70	3.24	4	416	~6	18.42±2.48	1810±0.03	2.34±0.27
SSC40-5	57.56	38.37	4.06	5	409	~5	20.25±2.66	1800±0.05	2.34±0.21

† Values were obtained as explained in the experimental section. Suspensions were prepared by dispersing powder mixtures of 60 wt.% β-$Si_4Al_2O_2N_6$ + 40 wt.% fused silica in NCPM (non-convectional premix) solution using 10 µL Dolapix CE 64 dispersing agent per gram of powder mixture.

* Formed upon hydrolysis and firing of added A-AlN

‡ In sample codes, SSC40 indicates the ceramic composite formed from a powder mixture of 60 wt.% β-$Si_4Al_2O_2N_6$ + 40 wt.% fused silica; the numbers 1-5 represent the AlN content equivalent to 1-5 wt.% Al_2O_3 on total powder basis added to the suspensions; A-AlN stands for as purchased AlN powder, which was not passivated against hydrolysis

powder mixture of 60 wt.% β-$Si_4Al_2O_2N_6$ and 40 wt.% fused silica; the numbers 1–5 represent the content of AlN added (equivalent to 1–5 wt.% Al_2O_3) into the slurry on total powder weight percent basis; A-AlN stands for as purchased AlN powder that was not passivated against hydrolysis. The viscosity of the slurries considerably decreased with the increasing concentrations of AlN in the slurry reaching the lowest value of 406 mPa s for SSC40-5. Usually, when AlN is introduced into aqueous slurry the following three reactions (equations (1-3)) take place.

$$AlN + 2H_2O \rightarrow AlO(OH) + NH_3 \quad (1)$$

$$NH_3 + H_2O \rightarrow NH_4OH \quad (2)$$

$$AlO(OH) + H_2O \rightarrow Al(OH)_3 \quad (3)$$

It consumes water, releases ammonia, and forms aluminium hydroxides. This released ammonia changes the pH and rheological characteristics of aqueous slurries [29,59]. In the present case, the generated ammonia gas increases the pH of the slurry away from the iso-electric-point of the dispersed powders thereby increases the stability and fluidity of slurry by decreasing their viscosities [29,59]. The slurry, SSC40-1, took about 11 minutes for completely converting into a gel after introducing APS, TEMED and AlN equivalent to 1 wt.% of Al_2O_3. On the other hand, the slurry, SSC40-5, took only about 5 min after introducing APS, TEMED and AlN equivalent to 5 wt.% of Al_2O_3. These results indicate that AlN concentration in the slurry drastically reduces the setting time of slurries under ambient conditions [29]. In all three events (equations 1-3), water is consumed and solids content is increased. These events support the early setting of slurries when higher amounts of AlN are introduced into them [19,59]. The flexural strength of green bodies also increased with the AlN content. In GCHAS process, strength not only comes from polymerization of organic monomers present in the slurry but also by the cementing action of boehmite formed by the hydrolysis of AlN added to the slurry [19,21,29,59]. The generated boehmite connects the ceramic particles into a stiff body and the content of this boehmite increases with the concentration of AlN in the slurry [29]. Due to the involvement of both strengthening mechanisms, the green SSC40-5 consolidates exhibited the highest green strength value of 20.25±2.66 MPa.

A gradual decrease in the values of green density (from 2830 to 2800 kg/m^3) and a gradual increase in the values of percentage linear shrinkage (from 2.32 to 2.34%) with the increasing AlN concentration in slurry can be seen from the data of Table 9. The decrease of green density with the increase of AlN concentration in the slurry could be attributed to the amount of NH_3 gas released in the slurry due to AlN hydrolysis (equation 1). Normally, some of the ammonia gas remains entrapped in the slurry having a viscosity of >400 mPa s, even after vacuum pumping. This entrapped gas leads to the formation of fine pores in the green bodies, which in turn are responsible for lower densities of consolidates. Nevertheless, these green density values are well-comparable with the one (2820 kg/m^3) measured for consolidate formed by CDPP route having the same composition of β-$Si_4Al_2O_2N_6$ and fused silica (SSC40).

The SSC40 consolidated by CDPP route followed by sintering for 3 h at 1750°C exhibited a bulk density of 2510 kg/m^3, apparent porosity of 5.445%, water absorption capacity of 2.168%, linear shrinkage of 10.68%, hardness of 1319 kg/mm^2, fracture toughness of 3.22 MPa m$^{1/2}$, and flexural strength of 113 MPa. On the other hand, the pure stoichiometric β-$Si_4Al_2O_2N_6$ formed

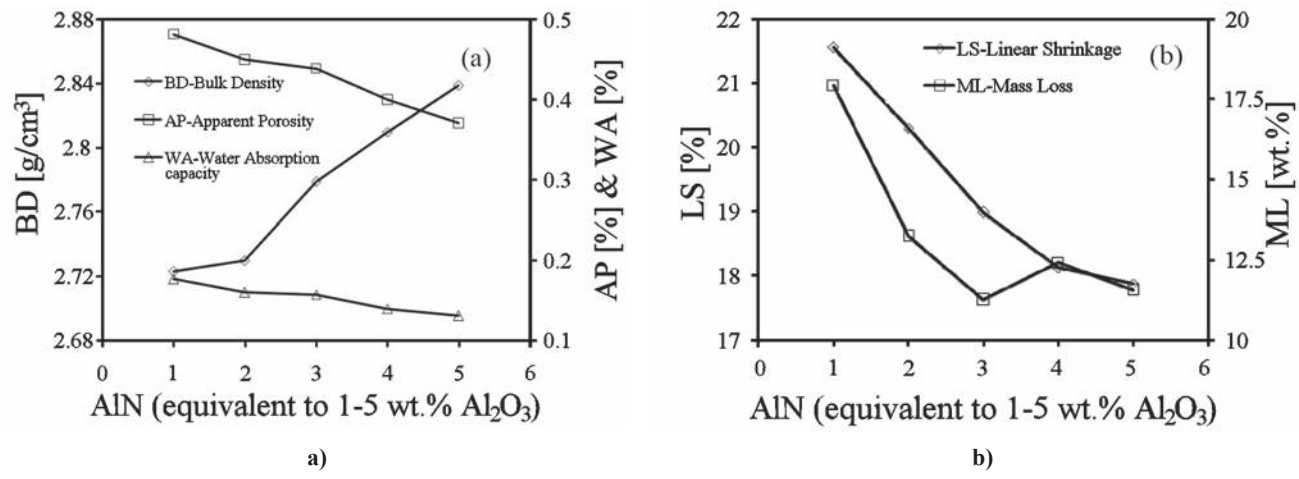

a) b)

Figure 14. (a) Bulk density (BD), apparent porosity (AP) and water absorption capacity (WA), and (b) linear shrinkage (LS) and mass loss (ML) of SSC40-1 to SSC40-5 sintered for 3 h at 1750°C (Table 9) [21]

by the reaction sintering (at 1675°C for 4 h) of extrudates consisting α-Si_3N_4, α-Al_2O_3, surface passivated AlN against hydrolysis and Y_2O_3 (7 wt.%) exhibited a bulk density of 3080 kg/m^3, apparent porosity of 0.19%, water absorption capacity of 0.12%, linear shrinkage of 14%, hardness of 1317 kg/mm^2, fracture toughness of 3.30 MPa m$^{1/2}$, and flexural strength of 216 MPa. Although the hardness and fracture toughness values of these two differently sintered materials are comparable, there is a large gap between their flexural (4-point bend) strength values (β-$Si_4Al_2O_2N_6$ had a strength 226 MPa, whereas, the SSC40, Si_2N_2O, had only about 113 MPa). The kinds of bonds and the amounts of porosity present in them could be responsible for the measured different flexural strength values [23].

The values of bulk density, apparent porosity and water absorption capacity, and the values of linear shrinkage and mass loss of SSC40-1 to SSC40-5 sintered for 3 h at 1750°C are plotted in Fig. 14a,b, respectively. Their corresponding hardness and fracture toughness values, and the flexural strength and Young's modulus values are plotted in Fig. 15a,b, respectively, as a function of the amount of AlN added to their corresponding slurries. In general, all these properties ap-

Table. 10. Sintered properties of SSC40-5 and of various commercial radome materials [21]

Materials trade ad manufacturers†	Basic chemical composition	BD [kg/m^3]	Elastic modulus [GPa]	Flexural strength [MPa]	CTE [10^{-6}/°C]	Dielectric permittivity [ε']	tan δ	Ref.
Pyoceram 9606 (Corning Inc., USA)	Cordierite	2600	121	240	4.7	5.5	0.0005	[3]
Fused silica (Ceradyne, Inc., USA)	SiO_2	2000	37	43	0.7	3.3	0.003	[2]
IRBAS (Lockheed Martin Inc., USA)	Si_3N_4	3180	280	550	3.2	7.6	0.002	[78]
Ceralloy 147-31N (Ceradyne, Inc., USA)	Si_3N_4	3210	310	800	-	8	0.002	[78]
Ceralloy 147-01EXP (Ceradyne, Inc., USA)	Reaction bonded Si_3N_4	1800-2500	50-200	180	3.1	4-6	0.002-0.005	[78]
β-SiAlON (ORNL, USA)	β-$Si_4Al_2O_2N_6$	3020	230	260	4.1	7.4	0.003	[3,6]
Cerablak™, (Applied Thin Films, Inc., USA)	Al_2O_3-P_2O_5 composite	2000-2500	-	-	5.0	3.3-5	-	[10]
Invisicone (AMO, USA)	β-SiAlON-SiO_2	2200	-	532	2.0	4.9	0.002	[4]
SSC40-5 (material of this study, Table 8)	Si_2N_2O	2810	214	140	3.50	5.896	0.002-0.003	-

† ORNL stands for Oak Ridge National Laboratory and AMO stands for Advanced Materials Organization; CTE-coefficient of thermal expansion; BD-bulk density.

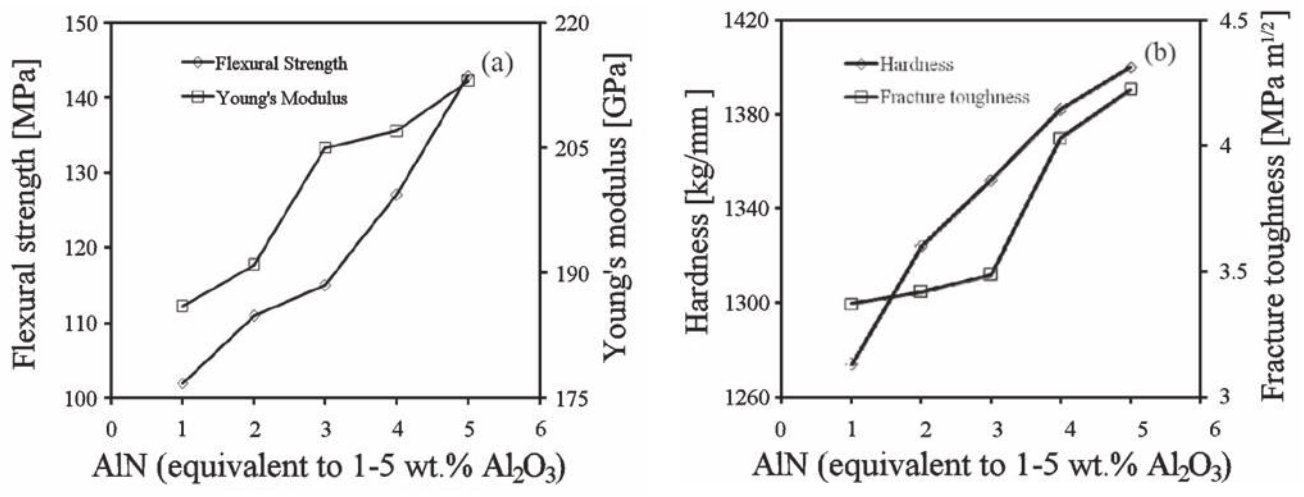

a) b)

Figure 15. (a) Hardness and fracture toughness, and (b) flexural strength and Young's modulus of SSC40-1 to SSC40-5 sintered for 3 h at 1750°C (Table 9) [21]

pear to be very sensitive to the AlN concentration in the slurries. There is a significant difference between the apparent porosity and water absorption capacity values measured for SSC40, and SSC40-1 to SSC40-5, though all these samples have been sintered under identical conditions. Furthermore, there is a gradual increase in the values of bulk density, hardness, fracture toughness, flexural strength and young's modulus, and a concurrent decrease in the values of apparent porosity, water absorption capacity, linear shrinkage and mass loss of SSC40-1 to SSC40-5 with the increasing concentration of AlN in the slurry. There is an increase in the values of hardness from 1270 to 1390 kg/mm^2, of fracture toughness from 3.35 to 4.2 MPa m$^{1/2}$, of flexural strength from 90 to 140 MPa and of Young's modulus from 184 to 213 GPa, and there is a decrease in the values of linear shrinkage from 22.5 to 18% and in the mass loss from 18 to 11%. The increased amounts of new alumino-silicate chemical bonds formed by the reactions between aluminium hydroxides derived from AlN and the Si_2N_2O (Fig. 13) could be responsible for the above mentioned changes in the sintered properties of SSC40-1 to SSC40-5.

Table 10 presents the basic chemical composition, bulk density, elastic modulus, flexural strength, co-efficient of thermal expansion, dielectric permittivity, and *tan δ* of SSC40-5 (Table 9) and of several other commercial radome materials. Materials trade names as well as the suppliers and their corresponding countries names are also summarized in this table. In general, all the radome materials exhibit reasonably low bulk density values (<3200 kg/m^3), which are recommended for high-speed radome materials. It can be seen that among various materials, only the Si_3N_4 and β-SiAlON based materials exhibit higher elastic modules and flexural strength values [79]. Except Cerablak™ (5.0×10^{-6}/°C), Pyroceram 9606 (4.7×10^{-6}/°C) and β-SiAlON (4.1×10^{-6}/°C), all other materials exhibited relatively low CTE values (<3.5×10^{-6}/°C). As far as the important dielectric permittivity property is concerned, the fused silica appears to be best for as it has the value of only 3.3. The highest permittivity values are measured for β-SiAlON (7.4), and the Si_3N_4 based materials, IRBAS (7.6) and Ceralloy 147-31N (8) [79]. Nevertheless, all these materials exhibited considerably low *tan δ* values (i.e. <0.003). When compared with other materials, the SSC40-5 possesses elastic modulus and flexural strength values that are almost three times higher than those of fused silica. The dielectric permittivity value of SSC40-5 was measured to be 5.896, which is less than that of β-$Si_4Al_2O_2N_6$ (7.4), IRBAS (7.6) and Ceralloy 147-31N (8). Based on these permittivity and strength properties together with the high temperature (>1300°C) withstanding and radome shape forming capability, this SSC40-5 can be considered for certain high speed radome applications [1–15].

IV. Conclusions

The following conclusions can be drawn from the above study:

1. Different types of dense β-$Si_{6-z}Al_zO_zN_{8-z}$ (z = 1, 1.5, 2, 2.5, 3, 3.5 & 4) ceramics can be prepared following a conventional reaction sintering process at 1675–1700°C for 4 h under ~800 torr N_2 pressure using α-Si_3N_4, α-Al_2O_3, AlN and Y_2O_3 (3, 5 & 7 wt.%) as starting materials.
2. An increase in z value and sintering aid (Y_2O_3) concentration can cause an increase in bulk density, co-efficient of thermal expansion, grain size, fracture toughness, dielectric constant and phase formation of β-$Si_{6-z}Al_zO_zN_{8-z}$ and as a consequence, the decrease of apparent porosity, water absorption capacity, hardness, 3-point bend strength.

3. A β-$Si_4Al_2O_2N_6$ ceramic formed at 1675°C for 4 h exhibits a bulk density of ~3067 kg/m^3, AP of ~0.012%, WA capacity of ~0.004%, XRD phase of ~94.43%, ~1317 kg/mm^2, fracture toughness of ~3.30 MPa.m$^{1/2}$, 3-point bend strength of ~226 MPa, coefficient of thermal expansion of 3.628 ×10^{-6}/°C between 30–700°C, and a dielectric constant of ~7.206 at 17 GHz. Furthermore, this material can also be prepared in the form of powder following a conventional extrusion process using the same precursor mixture in which the surface passivated AlN against hydrolysis needs to be utilized as one of the starting raw materials.
4. AlN powder can be successfully passivated against hydrolysis just by treating it in an ethanolic solution containing required amounts of ortho-phosphoric acid and aluminium di-hydrogen phosphate at 80°C for 24 h.
5. Dense ceramics of β-$Si_4Al_2O_2N_6$ can also be consolidated following various colloidal processing routes such as, aqueous gelcasting, hydrolysis assisted solidification and hydrolysis induced aqueous gelcasting (GCHAS) routes. Among various colloidal processing routes employed, the GCHAS was found to be superior for making thin wall β-$Si_4Al_2O_2N_6$ radomes and crucibles. Further, these green radome structures can be densified fully without the distortion of shape by following the conformal sintering and can be machined to obtain the desired finish using diamond tools.
6. Dense ceramic composites of β-$Si_4Al_2O_2N_6$-fused silica with SiO_2 in the range of 20–80 wt.% can be prepared by sintering the dry-powder pressed composites of β-$Si_4Al_2O_2N_6$ and fused silica for 3-4 h at 1500–1750°C.
7. The Si_2N_2O formed at 1750°C for 3 h from a powder mixture of 60 wt.% β-$Si_4Al_2O_2N_6$ and 40 wt.% fused silica exhibits flexural strength value more than three times of sintered bulk fused silica, and the dielectric constant value less than that of stoichiometric β-$Si_4Al_2O_2N_6$.

Acknowledgements: Author thanks Dr. G. Sundararajan, Director, ARCI for his kind encouragement while writing this manuscript and for his kind permission to publish this article. He also expresses his gratitude to his colleagues at ARCI for their contributions to this study.

References

1. D.G. Paquette, "Method of making a radar transparent window material operable above 2000°C", *U.S. Patent No,* 5,627,542, May. 6, 1997 (*and references therein*).
2. M.A. Janney, C.A. Walls, D.M. Kupp, K.W. Kirby, "Gelcasting SiAlON radomes", *Am. Ceram. Soc. Bull*., July (2004) 9201–9206.
3. K.W. Kirby, A.T. Jankiewicz, M.A. Janney, C. Walls, D. Kupp, "Gelcasting of GD-1 ceramic radomes", pp. 287–295 in *Proceedings of the 8th DoD Electromagnetic Windows Symposium*. U.S. Airforce Academy, Boulder, Colorado Springs, April 2000.
4. K.W. Kirby, A. Jankiewicz, D. Kupp, C. Walls, M.A. Janney, "Gelcasting of ceramic radomes in the Si_3N_4-Al_2O_3-AlN-SiO_2 system", *Mater. Tech. & Adv. Perf. Mater.*, **16** [3] (2001) 187-190.
5. K.W. Kirby, A.T. Jankiewicz, R.F. Lowell, R.L. Hallse, "Near net shape fabrication of ceramic radomes", *U.S. Patent No,* 6,083,452, July 4, 2000.
6. G. Gilde, P. Patel, C. Hubbard, B. Pothier, T. Hynes, W. Croft, J. Wells, "SiON low dielectric constant ceramic nanocomposite", *U.S. Patent No,* 5,677,252, Oct. 14, 1997.
7. J.T. Neil, L.J. Bowen, B.E. Michaud, "Fused silica radome", *U.S. Patent No,* 4,949,095, August 14, 1990.
8. D.W. Freitag, K.K. Richardson, "BAS reinforced in-situ with silicon nitride", *U.S. Patent No*, 5,358,912, Oct. 25, 1994.
9. I.G. Talmy, D.A. Haught, "Ceramics in the system $BaOAl_2O_32SiO_2$-$SrOAl_2O_32SiO_2$ as candidates for radomes", *Technical Report*, Contract N60921-8-R-0200, Naval Surface Warfare Centre, 1989.
10. F.G. Mora, K.C. Goretta, D. Singh, J.L. Routbort, S. Sambasivan, K.A. Steiner, J. Adabie, K.K. Rangan, "High-temperature deformation of amorphous Al-PO_4-based nano-composites", *J. Eur. Ceram. Soc*., **26** (2006) 1179–1183.
11. Y. Wang, J. Liu, "Aluminium phosphate-mullite composites for high-temperature radome applications", *Int. J. Appl. Ceram. Technol*., **6** [2] (2009) 190–194.
12. J. Wu, J. Guo, B. Li, "Preparation and properties of SiO_2 matrix composites doped with AlN particles", *J. Mater. Sci*., **35** [19] (2000) 4895–4900.
13. G. Wen, G.L. Wu, T.Q. Lei, Y. Zhou, Z.X. Guo, "Co-enhanced SiO_2-BN ceramics for high-temperature dielectric applications", *J. Eur. Ceram. Soc*., **20** [12] (2000) 1923–1928.
14. M.Y. Hsieh, "Silicon nitride having low dielectric loss", *U.S. Patent No*, 4,642,299, February 10, 1987.
15. M.Y. Hsieh, H. Mizuhara, P.W. Smith, "Pressureless sintered silicon nitride as a promising candidate for radome materials", 17th Symposium on electromagnetic windows, Atlanta Ga., July 25-27, 1984.
16. L. Edward, F.H. Simpson, J.F. Schorsch, "Broadband high temperature radome apparatus", *U.S. Patent No*, 4,677,443, Jun. 30, 1987.
17. H. Leggett, "Ceramic broadband radome", *U.S. Patent No*, 4,358,772, Nov. 9, 1982.
18. I. Ganesh, N. Thiyagarajan, D.C. Jana, P. Barik, G. Sundararajan, "An aqueous gelcasting route to dense β-$Si_4Al_2O_2N_6$-0.5SiO_2 ceramics", *J. Am. Ceram. Soc*., **91** [5] (2008) 1566–1571.
19. I. Ganesh, "Near-net shape β-$Si_4Al_2O_2N_6$ parts by hydrolysis induced aqueous gelcasting process", *Int. J. Appl. Ceram. Technol*., **6** [1] (2009) 89–101.

20. I. Ganesh, N. Thiyagarajan, D.C. Jana, Y.R. Mahajan, G. Sundararajan, "An aqueous gelcasting process for β-$Si_4Al_2O_2N_6$ ceramics", *J. Am. Ceram. Soc*., **91** [9] (2008) 3121–3124.
21. I. Ganesh, G. Sundararajan, "Hydrolysis induced aqueous gelcasting of β-SiAlON-SiO_2 ceramic composites: the effect of AlN additive", *J. Am. Ceram. Soc*., **93** [10] (2010) 3180–3189.
22. M.A. Janney, S.D. Nunn, C.A. Walls, O.O. Omatete, R.B. Ogle, G.H. Kirby, A.D. McMillan, "Gelcasting"; pp. 1–15 in *The Handbook of Ceramic Engineering*. Edited by M.N. Rahman, Marcel Dekker, New York, 1998.
23. S. Hampshire, H.K. Park, D.P. Thompson, H.K. Jack, "α-SiAlON", *Nature*, **274** (1978) 880–882.
24. I. Ganesh, N. Thiyagarajan, D.C. Jana, Y.R. Mahajan, G. Sundararajan, "Influence of chemical composition and Y_2O_3 on sinterability, dielectric constant and CTE of β-SiAlON", *J. Am. Ceram. Soc*., **91** [1] (2008) 115–120.
25. T. Kosmac, S. Novak, M. Sajko, "Hydrolysis-assisted solidification (HAS): a new setting concept for ceramic net-shaping", *J. Eur. Ceram. Soc*., **17** (1997) 427–432.
26. I. Ganesh, G. Sundararajan, "A novel route to β-SiAlON-SiO_2 ceramic composites", *Adv. Appl. Ceram.*, **110** [2] (2011) 87–94.
27. Y. Shimizu, J. Hatano, T. Hyodo, M. Egashira, "Ion-exchange loading of yttrium acetate as a sintering aid on aluminum nitride powder via aqueous processing", *J. Am. Ceram. Soc*., **83** [11] (2000) 2793–2797.
28. K. Krnel, T. Kosmac, "Reactivity of aluminum nitride powder in dilute inorganic acids", *J. Am. Ceram. Soc*., **83** [6] (2000) 1375–1378.
29. K. Krnel, T. Kosmac, "Protection of AlN powder against hydrolysis using aluminum dihydrogen phosphate", *J. Euro. Ceram. Soc*., **21** (2001) 2075–2079.
30. Y. Morisada, T. Sakurai, Y. Miyamoto, "A new water-resistant coating on AlN powder", *Inter. J. Appl. Ceram. Tech*., **1** [4] (2004) 374–380.
31. I. Ganesh, S.M. Olhero, A.A. Branca, M.R. Correia, G. Sundararajan, J.M.F. Ferreira, "Chemisorption of phosphoric acid and surface characterization of as passivated AlN powder against hydrolysis", *Langmuir*, **24** [10] (2008) 5359–5365.
32. I. Ganesh, N. Thiyagarajan, G. Sundararajan, S.M. Olhero, J.M.F. Ferreira, "A non-aqueous processing route for phosphate-protection of AlN powder against hydrolysis", *J. Eur. Ceram. Soc*., **28** (2008) 2281–2288.
33. Y. Oyama, O. Kamagaito, "Solid solubility of some oxides in Si_3N_4", *Jpn. J. Appl. Phys*., **10** (1971) 1637–1642.
34. K.H. Jack, W.I. Wilson, "Ceramics based on the Si-Al-O-N and related systems", *Nature*, *Phys. Sci.*, **238** (1977) 28–29.
35. K.H. Jack, "Review: SiAlONs and related nitrogen ceramics", *J. Mater. Sci*., **11** (1976) 1135–1158.
36. K.H. Jack, "Sialons: A Study in Materials Development"; pp. 1–30 in *Non-Oxide Technical and Engineering Ceramics*. Edited by S. Hampshire, Elsevier Applied Science Publishers Ltd., London, 1986.
37. I.W.M. Brown, G.C. Barris, M.E. Bowden, K.J.D. Mackenzie, C.M. Sheppard, G.V. White, "Synthesis, Densification, and Properties of SiAlON Bodies and Composites"; pp. 95–104 in *SiAlONs*. Edited by K. Komeya, M. Mitomo, Y.B. Cheng, Key Engineering Materials, Trans Tech Publications Ltd., Zurich, Switzerland, 2001.
38. X. Xu, M.I.L.L. Oliveira, F. Renli, J.M.F. Ferreira, "Effect of dispersant on the rheological properties and slip casting of concentrated SiAlON precursor suspensions", *J. Euro. Ceram. Soc*., **23** [9] (2003) 1525–1530.
39. S.J. Stedman, J.R.G. Evans, R.J. Brook, M.J. Hoffmann, "Anisotropic sintering shrinkage in injection moulding composite ceramics", *J. Euro. Ceram. Soc*., **11** [6] (1993) 523–532.
40. X. Xu, J.M.F. Ferreira, "Temperature-induced gelation of concentrated sialon suspensions", *J. Am. Ceram. Soc*., **88** [3] (2005) 593–598.
41. J.R.G. Evans, "Seventy ways to make ceramics", *J. Eur. Ceram. Soc*., **28** (2008) 1421–1432.
42. R.M. German, "R&D in support of powder injection molding: status and projections", *Inter. J. Powder Metallurgy*, **43** [6] (2007) 47–57.
43. R.M. German, "The scientific status of powder injection molding", *Inter. J. Powder Metallurgy*, **36** [3] (2000) 31–36.
44. R.M. German, R.G. Cornwall, "Summary report on the worldwide market and technology for injection moulding of metals and ceramics"; pp. 1831–1844 in *Advances in Powder Metallurgy and Particulate Materials, International Conference on Powder Metallurgy and Particulate Materials*, Chicago, IL; 1997.
45. J.R.G. Evans, J. Greener, "Elongational flow processing of ceramics", *J. Mater. Proc. Tech*., **96** (1999) 142–150.
46. R.E.F.Q. Nogueira, M.J. Edirisinghe, D.T. Gawne, "Selection of a powder for ceramic injection moulding", *J. Mater. Sci*., **27** [23] (1992) 6525–6531.
47. J.R.G. Evans, M.J. Edirisinghe, "Interfacial factors affecting the incidence of defects in ceramic mouldings", *J. Mater. Sci*., **26** [8] (1991) 2081–2088.
48. M.J. Edirisinghe, "The use of silane coupling agents in ceramic injection moulding: effect on polymer removal", *J. Mater. Sci. Lett*., **9** [9] (1990) 1039–1041.
49. M.J. Edirisinghe, "Solid freeform fabrication methods for engineering ceramics"; pp. 125–132 in *Better Ceramics Through Processing*, *Series - British Ceramic Processing **58***, Royal Agr Coll, Cirencester, England, 1998.
50. B.Y. Tay, J.R.G. Evans, M.J. Edirisinghe, "Solid free form fabrication of ceramics", *Inter. Mater. Rev*., **48** [6] (2003) 341–370.

51. J.D. Cawley, "Solid free form fabrication of ceramics", *Curr. Opin. Solid State Mater. Sci.*, **4** (1999) 483–489.
52. J. H. Song, M. J. Edirisinghe, J. R. G. Evans, E. H. Twizell, "Modelling the effect of gas transport on the formation of defects during thermolysis of powder mouldings", *J. Mater. Res*., **11** [4] (1996) 830–840.
53. SLS plastic prototypes for functional product testing, DTM corporation, 2001.
54. N.K. Tolochkesto, S.E. Mozzharov, N.V. Sobolenko, I.A. Yadroitsev, V.I. Goryushkin, V.S. Dubovets, "Problems and prospects of selective layer-by-layer laser sintering of powders", *Powder Metall. Met. Ceram.*, **34** [3-4] (1995) 142–145.
55. Z.H. Liu, J.J. Nolte, J.I. Packard, G. Himas, F. Dogan, M.C. Leu, "Selective laser sintering of high-density alumina ceramic parts", pp. 351–354 in *Proceedings of the 35th International MATADOR conference - Formerly the International Machine Tool Design and Research Conference*. National Editors S. Hinduja and K. C. Fan, University of Taiwan, Taipei, Taiwan, 2007.
56. I. Shishkovsky, I. Yadroitsev, P. Bertrand, I. Smurov, "Alumina-zirconia ceramics synthesized by selective laser sintering/melting", *Appl. Surf. Sci*., **254** [4] (2007) 966–970.
57. P. Bertrand, F. Bayle, C. Combe, P. Goeurit, I. Smurov, "Ceramic components manufacturing by selective laser sintering", *Appl. Surf. Sci*., **254** [4] (2007) 989–992.
58. I. Ganesh, "Hydrolysis induced aqueous gelcasting: a latest concept for net shape consolidation of ceramics (a review)", *Mater. Manufact. Process.*, DOI: 10.1080/10426914.2011.585494.
59. I. Ganesh, N. Thiyagarajan, D.C. Jana, P. Barik, G. Sundararajan, J.M.F. Ferreira, "Dense β-SiAlONs consolidated by a modified hydrolysis assisted solidification route", *J. Eur. Ceram. Soc*., **28** [4] (2008) 879–885.
60. I. Ganesh, S.M. Olhero, P.M.C. Torres, F.J. Alves, J.M.F. Ferreira, "Hydrolysis induced aqueous gelcasting for near-net shaping of ZTA ceramic composites", *J. Eur. Ceram. Soc*., **29** (2009) 1393–1401.
61. I. Ganesh, G.J. Reddy, G. Sundararajan, S.M. Olhero, P.M.C. Torres, J.M.F. Ferreira, "Hydrolysis induced aqueous gelcasting of $MgAl_2O_4$ spinel", *Int. J. Appl. Ceram. Technol*., **8** [4] (2011) 873–884.
62. I. Ganesh, G.J. Reddy, G. Sundararajan, S.M. Olhero, P.M.C. Torres, J.M.F. Ferreira, "Influence of processing route on micro-structure and mechanical properties of $MgAl_2O_4$ spinel", *Ceram. Int*., **36** (2010) 473–482.
63. I. Ganesh, G. Sundararajan, S.M. Olhero, P.M.C. Torres, J.M.F. Ferreira, "A novel colloidal processing route to alumina ceramics", *Ceram. Int*., **36** (2010) 1357–1364.
64. I. Ganesh, G. Sundararajan and J.M.F. Ferreira, "Aqueous slip casting and hydrolysis assisted solidification of $MgAl_2O_4$ spinel", *Adv. Appl. Ceram.*, **110** [2] (2011) 63–69.
65. I. Ganesh, S.M. Olhero, J.M.F. Ferreira, "A phosphoric acid treated AlN powder for aqueous processing of net-shape dense AlN and β-SiAlON parts", *Adv. Appl. Ceram.*, **108** [2] (2009) 111–117.
66. I. Ganesh, "Surface oxidation and dispersion behaviour of phenolic resin coated α-SiC powder in the aqueous medium", *Adv. Appl. Ceram.*, **107** [4] (2008) 210–216.
67. I. Ganesh, "Fabrication of near net shape magnesium aluminate ($MgAl_2O_4$) spinel components *via* aqueous processing", *Adv. Appl. Ceram.*, DOI: 10.1179/1743676110Y.0000000020.
68. B.P. Saha, R. Johnson, I. Ganesh, G.V.N. Rao, S. Bhattacharjee, Y.R. Mahajan, "Thermal anisotropy in sintered cordierite monoliths", *Mater. Chem. Phys.*, **67** [1-3] (2001) 140–145.
69. S. Brunauer, P.H. Emmett, E. Teller, "Adsorption of gases in multi molecular layers", *J. Am. Chem. Soc*., **60** (1938) 309–319.
70. H.P. Klug, L.E. Alexander, "X-ray diffraction procedure for polycrystalline and amorphous materials", *J. Appl. Crystallogr*., **8** (1975) 573–574.
71. G.R. Anstis, P. Chantikul, B.R. Lawn, D.B. Marshall, "A critical evaluation of indentation techniques for measuring fracture toughness. I. direct crack measurements", *J. Am. Ceram. Soc*., **64** (1981) 533–538.
72. A.M. Nicolson, G.F. Ross, "Measurement of the intrinsic properties of materials by time domain techniques", *IEEE Trans. Instrum. Meas.*, **IM-19** (1970) 377–382.
73. W.D. Kingery, H.K. Bowen, D.R. Uhlman, *Introduction to Ceramics*, 2nd Edn., Wiley, New York, 1976.
74. J.A. Dean, *Lange's Handbook of Chemistry*, 12th edn, McGraw-Hill, New York, 1979.
75. D.R. Lide, *CRC Hand Book of Chemistry and Physics*, 73rd Edn., CRC Press, London, 1993.
76. P. Pettersson, Z. Shen, M. Johnsson, M. Nygren, "Thermal shock properties of β-SiAlON ceramics", *J. Euro. Ceram. Soc*., **22** (2002) 1357–1365.
77. R.C. Buchanan, "Properties of ceramic insulators", *Chapter 1 in Ceramic Materials for Electronics, Processing, Properties and Applications*, 2nd Edn. Edited by R.C. Buchanan, Revised and Expanded, Marcel Decker Inc., New York, 1991.
78. V. Raghavan, "Dielectric materials", *Chapter 17, in Materials Science and Engineering – A First Course*, 4th Edn., Prentice-Hall of India (P) Ltd., New Delhi, 1998.
79. J. Mangels, B. Mikijelj, "Ceramic radomes for tactical missile systems"; http://www.cera dyne.com/uploads/Radome%20White%20Paper %20PDF.pdf, 2009.